EUROPEAN ORGANISATION FOR NUCLEAR RESEARCH

CERN – PS DIVISION

CERN/PS 98-063 (RF-HP)

REPORT OF THE STUDY GROUP ON A SUPERCONDUCTING PROTON LINAC AS A PS INJECTOR

D. Boussard*, R. Cappi, R. Garoby, H. Haseroth, C.E. Hill, P. Knaus,
A.M. Lombardi (ed.), M. Martini, P.N. Ostroumov**,
J.M. Tessier*, M. Vretenar (ed.)

Abstract

A proposal was made at the end of 1996 to use the large inventory of RF hardware available after the decommissioning of LEP-2 for the construction of a 2 GeV Superconducting Proton Linac (SPL) to inject directly into the PS [1.1]. The brightness of the beam in the PS at low energy would double, helping the injector complex to satisfy the requirements of the LHC and benefiting the planned proton physics programme. Additional users could also be accommodated thanks to the capability of the SPL to operate at a much larger duty factor than that required for high-energy physics. Consequently, a small study group has been set up to analyse the major technical aspects of the SPL design as well as the processes of injection and capture in the PS. This report summarises the work done so far, and provides some information about the other possible uses of the SPL beam. The feasibility of such a cascade of accelerators is confirmed, although an in-depth design study is still required before the realistic performance and detailed design of that facility can be announced.

* SL Division
** INR, Moscow, Russia

Geneva, Switzerland
3 December 1998

TABLE OF CONTENTS

1 INTRODUCTION

As a result of the decommissioning of the lepton collider, most of the RF equipment of LEP-2 (Table 1.1) will be available after the year 2000. Among the possible new uses of this expensive hardware [1.2-1.5] is the attractive option [1.1] of a 2 GeV linac injector for the PS. Such a linac offers the following benefits with respect to the present scheme for the LHC era [1.6]:

- The brightness of the proton beam (number of protons per unit of transverse emittance) delivered by the PS injector complex is improved, which helps the reliable generation of the beams for the LHC. Due to the 2 GeV injection energy into the PS, the brightness can be multiplied by 1.6 while keeping a similar space charge-induced tune spread as compared with 1.4 GeV.
- There is the potential to improve other characteristics of the PS beam, like peak intensity. Since beam brightness can be increased, the total beam current can also be increased by filling the available aperture.
- Beam losses are reduced with the charge exchange injection process in the transverse planes and with the direct capture of the chopped linac beam in the longitudinal phase plane.
- The injectors of the PS are modernised and built with highly standardised equipment, increasing reliability and easing maintenance.
- New users can be accommodated using the capability of the linac to operate at a high duty factor (1 MW beam power at 2 GeV is potentially available with a 5% duty factor).

Frequency	352.209 MHz
Number of modules (4 cavities per module)	68
Maximum voltage per module (E=6 MV/m and β=1)	40 MV
R/Q	232 Ω
Power rating of the RF coupler	120 kW
Total number of 1 MW (CW) klystrons	44
Cryogenic power at 4.5 K [1.7] (~1/3 for static losses and 2/3 for dynamic RF load)	4 x 10 kW

Table 1.1: Basic parameters of the LEP-2 RF hardware [1.4, 1.7].

Given the limited effort available, the work of the study group has concentrated on the most promising scenario described in Section 2. For this scheme, the main issues concerning accelerator technology have been covered (Sections 3 and 4). These include:

- the H^- source, as compared with existing and planned H^- sources world-wide,
- a preliminary design of a room-temperature 100 MeV linac incorporating a wide-band chopper between two RFQ structures,
- the results from on-going research and development on the application of the niobium sputtering technique to the fabrication of so-called “reduced-beta” (β<=0.8) superconducting (SC) cavities,

- a preliminary investigation of the beam dynamics of a 100 MeV - 2 GeV SC linac section using 352 MHz RF structures inside LEP-2 cryostats,
- an analysis of the energy stability of the 2 GeV beam in the presence of microphonic detuning of the cavities,
- a design of the debunching section at the end of the linac,
- a first design and simulation of charge exchange injection into the PS at 2 GeV,
- an analysis by simulation of the longitudinal capture in the PS taking longitudinal space charge into account.

The general conclusion of this study is that such a machine is feasible, although not all technical questions have necessarily been given the optimum answer. More work is required to refine some parameters. In particular, further studies are necessary to define the optimum transfer energy between room-temperature and SC RF, the maximum accelerating gradient in the LEP-2 cavities in pulsed mode and the best construction method for reduced-beta SC cavities.

Important domains like cryogenics, layout on the CERN site and infrastructure (controls etc.) have not been studied , but none of these is likely to change the conclusion of the feasibility of the accelerator. However, they must be subject to proper investigation before beginning any serious cost analysis. The options of re-using the existing 50 MeV Alvarez linac or using the LEP cavities in a mode different from π, which were considered at the beginning of the study [1.1], have been discarded because of their complexity and the performance limitations they introduce.

Given the size of such a linac, another important task was to consider the interest of some new potential uses. Profiting from the capability to operate at a higher duty cycle than that required by the present proton users at CERN, an upgraded ISOLDE could be supplied with much more beam current (up to 1 mA), or a neutron spallation source could be built to receive up to 1 MW beam power on target. Due to the improved beam characteristics, a higher beam intensity can be delivered by the PS for the needs of experimental physics (neutrino experiments) and interesting machine physics studies towards the design of future accelerators, like the proton driver for a muon collider, can be carried out. The outcome of these investigations is summarised in Section 5.

2 CHOICE OF PARAMETERS AND OVERALL LAYOUT

The main SPL parameters are summarised in the Table 2.1. The SPL comprises an H^- source, two RFQs with a chopper in between, a Drift Tube Linac (DTL) which takes the beam up to 100 MeV and a SC section up to the final energy of 2 GeV. The schematic layout of the SPL is shown in Figure 2.1.

Linac Current

The design foresees 1.4×10^{13} particles at the exit of the PS. This corresponds to the LHC beam-beam limit (the so-called "ultimate beam"). H^- ions are accelerated in the SPL and charge exchange injection is used in the PS to minimise injection losses and the transverse emittance of the accumulated beam. The mean SPL current has been fixed at 10 mA, which means that the required number of particles can be obtained with an SPL pulse length of ~250 μs by injecting 110 turns in the PS. With a PS repetition period of 1.2 s, the SPL beam duty cycle for LHC is only 0.021%.

The mean SPL current of 10 mA is the result of a compromise between many factors. A lower mean current and a proportionally longer beam pulse reduces the number of klystrons needed by the SC section, but increases the complexity of the power distribution network and the number of turns required at injection in the PS. A higher current improves the power efficiency of the Room Temperature (RT) section and reduces the number of turns injected in the PS. However, it also leads to space charge problems at low energy and to an increase of the RF power driving the SC section, which implies a larger number of klystrons and is finally limited by the maximum power handling capability of the RF windows. Moreover, for 10 mA current no modifications are required to the input couplers of the LEP-2 cavities.

For the design mean current, the H^- source has to deliver about 20 mA, which is within the capabilities of existing ion sources.

Energy

The PS injection energy should be as high as possible to reduce the incoherent betatron oscillation tune shift $\Delta Q \propto 1/\beta\gamma^2$ induced by space charge. At the same time, the transit time factor of the existing LEP-2 cavities goes up with particle velocity, making the SPL more efficient at high energy. The linac energy is therefore mainly decided by the amount of material that can be recuperated from LEP and by cost considerations. For the present study an energy of 2 GeV is assumed, easily reached by using most of the LEP-2 equipment. At 2 GeV the tune shift at PS injection would be reduced by a factor 1.6 as compared to the present injection at 1.4 GeV.

RF Frequency

A standard RF frequency is a clear advantage in terms of cost and maintenance. For this reason, the LEP RF frequency of 352.2 MHz used for the SC part of the linac has been adopted as well for most of the RT part.

a. Main Beam Parameters

No. injected particles per PS pulse	1.5	10^{13}	LHC beam-beam limit
Mean current during pulse	10	mA	
Pulse length	250	μs	110 PS turns
Repetition rate	0.83	Hz	1.2 s between pulses
Linac filling factor	1/2		every other bucket filled
No. linac bunches per PS bucket	11		for lossless capture in the PS
SPL Micropulse	59.6	ns	equivalent to 11 linac bunches
Chopping factor	46	%	chopped beam on total
Mean bunch current	37	mA	in an RF period, for full buckets
Source current	20	mA	
Beam duty cycle (for LHC)	0.021	%	
Maximum design duty cycle	5	%	for possible other applications
Maximum average current	500	μA	5% duty cycle

b. Transverse Emittance Budget (μm, rms, normalised)

	in	out
Source		0.2
RFQs + chopper	0.2	0.3
DTL	0.3	0.4
SC section	0.4	0.6
PS	0.6	1.5

c. Longitudinal Plane

	SC exit	PS input		
Emittance	3	3	π ° MeV	total (5 rms)
Energy spread	±2	±0.5	MeV	total (√5 rms)
Phase spread	±1.5	±10	deg at 352 MHz	total (√5 rms)
Energy jitter	±6	±1.2	MeV	total, from microphonics

d. Linac Sections

	Freq. [MHz]	W_{in} [MeV]	W_{out} [MeV]	Description
Source	-		0.05	
RFQ1	176.1	0.05	2	
chopper	-	2	2	wide-band electrostatic chopper
RFQ2	352.2	2	7	
DTL1	352.2	7	20	standard Alvarez tank
DTL2	352.2	20	100	SDTL (tanks with external quadrupoles)
SC1	352.2	100	1000	reduced-beta SC cavities
SC2	352.2	1000	2000	standard LEP2 cavities
Transfer line		2000	2000	200 m “debunching” line

Table 2.1: Main SPL Parameters.

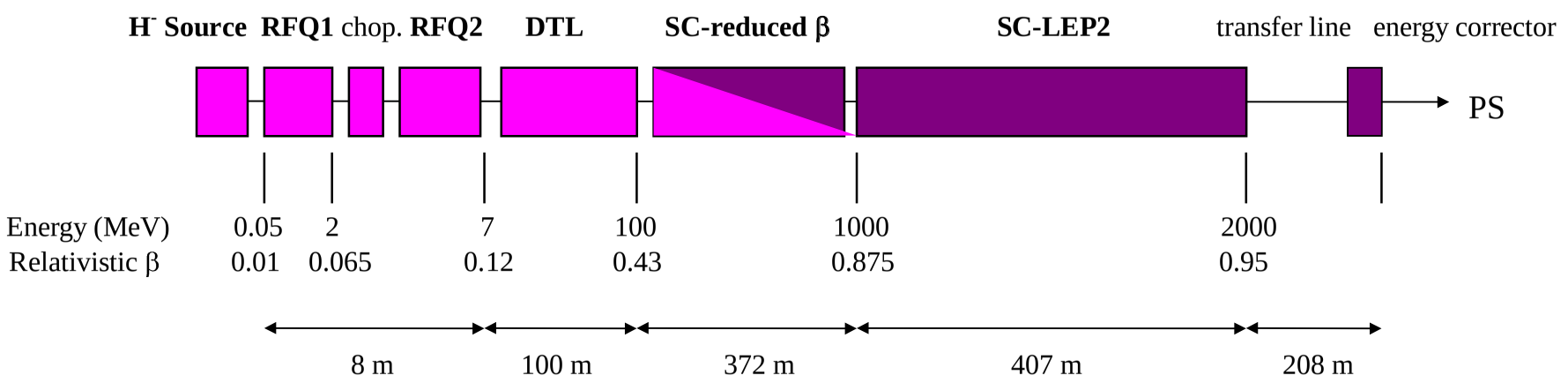

		Win [MeV]	Wout [MeV]	Freq. [MHz]	No. Cavities	Power [MW]	No. Klystrons	Length [m]
1	RFQ1	0.05	2	176.1	1	0.45	-	2.3
2	RFQ2	2	7	352.2	1	0.5	1	4
3	DTL	7	100	352.2	29	5.8	6	99
4	SC - reduced β	100	1027	352.2	152	13	19	372
5	SC - LEP 2	1027	2000	352.2	136	14.2	17	407
6	Transfer line	2000	2000	352.2	1		-	208
	Total						**43**	**1094**

Figure 2.1: Schematic layout of the SPL. A darker shadow indicates elements that can be recuperated from LEP.

Chopping

In order to achieve a high longitudinal capture efficiency, an essential feature of the SPL is the chopping of the linac beam at the PS RF frequency. Chopping is provided at 2 MeV by a wide-band electrostatic chopper, similar to the one used at BNL [2.1], placed between two RFQs. The frequency of the first RFQ (RFQ1), a sub-harmonic of the main linac frequency, defines the rise-time of the chopper, which must be shorter than the time between two bunches, while the linac filling factor (fraction of full buckets) determines the mean bunch current. In the basic design, a compromise has been made assuming a frequency of 176 MHz for RFQ1. This corresponds to a chopper rise-time of 4.2 ns and a filling factor of a half, which keeps the mean bunch current, defined over one cycle at 352 MHz, to less than 40 mA. This solution, however, requires the development of a fast chopper with a rise-time more than a factor of two smaller than the BNL device. The chopper is also used to produce an empty interval for the rise-time of the ejection kicker, eliminating one complete linac micropulse per PS revolution period (2.212 μs). The number of linac bunches that fall inside the PS bucket, 11 in the preferred scenario, and the 1/21 ratio of missing pulses for ejection define the chopping factor (beam-off time on total) to 46%. The resulting mean bunch current is 37 mA. The time structure of the SPL beam is sketched in Figure 2.2.

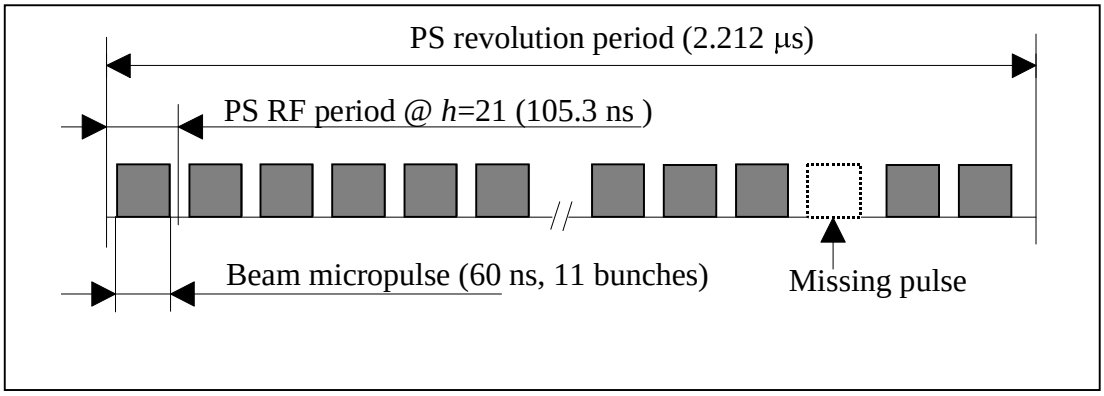

Figure 2.2: Time structure of the SPL beam pulse at injection in the PS.

Pulsing of SC Cavities and Duty Cycle

Since the SPL duty cycle required in the "PS for LHC" scenario is only 2×10^{-4}, the SC cavities need to be pulsed to minimise heat dissipation in the structures and average power consumption. The pulsing of SC RF systems is a field where some development has been done recently by the TESLA collaboration [2.2] and a specific approach for the SPL is described in Section 3.2.4. Up to a duty cycle of about 5%, the size of the cryogenic system is mainly determined by static losses and RF pulsing has no impact on the required power of the cryoplants. Some precautions in the design of the cooling systems for the RT section have to be taken in order to have a linear accelerator that can operate at 5% duty cycle, for example with 1 ms pulses at 50 Hz. However, an important additional overhead incurred for a 5% duty cycle is the shielding needed to cope with the higher activation due to losses in the SPL.

Transverse Emittance

An important design constraint of the SPL is the minimisation of the transverse emittance, which should be smaller than that of the present 50 MeV beam injected into the PSB. A possible transverse emittance budget is shown in Table 2.1b. The H^- source emittance of 0.2 μm (rms, normalised) is well within present capabilities, while a blow-up of 100% has been pessimistically assumed in the RT section due to space charge effects, mismatch between the different sections and misalignments. Another 50% blow-up has been conservatively assumed for the SC section, with misalignment the main source. The simulations of injection in the PS have thus been made painting the PS acceptance with an emittance of 0.6 μm to allow for this overall blow-up by a factor of three from source to PS. For comparison, the present high current Linac2 injector (180 mA, 50 MeV) shows a blow-up of a factor two between source and PSB injection, predicted by the simulations and mainly due to space charge effects.

Beam Losses and Halo Formation

A major concern of high energy linac designs is the activation due to beam losses. In the case of the SPL, the loss limit of 1 W/m for hands-on maintenance [2.3] corresponds to a relative particle loss at 2 GeV of 10^{-4}/m for the nominal (LHC only) duty cycle and of 10^{-6}/m for the 5% maximum duty cycle. The latter is between one and two orders of magnitude higher than for projects like ESS or APT which have mean beam powers correspondingly higher [2.4, 2.5]. In the SPL, space charge related halo formation would be minimal due to the low mean bunch current of 37 mA. In addition, the large ratio between aperture and rms beam radius in the SC cavities, which is between 35 and 75 in the present design, allows most of the halo particles to be transported and properly removed on collimators before PS injection. However, the issue of beam losses is considered important enough to require further detailed analysis of halo formation in the SPL and some modifications to the design, like a more gradual change of the focusing period between the linac sections.

Other Options

The transition energy between RT and SC parts has been preliminarily fixed to 100 MeV. However, in case the sputtering of niobium on the lowest beta superconducting cavities would not be feasible, they would be made of bulk niobium and the DTL energy increased up to 150 MeV.

A scheme based on the re-utilisation of the 50 MeV Linac2 as an injector for a 352 MHz linac has been considered [2.6] and discarded, at least for the time being. It would involve the replacement of the present RFQ of Linac2 with a new one operating at 50.3 MHz (i.e., 1/7th of the SC frequency) and the re-tuning of Linac2 from 202.56 MHz to 201.3 MHz. This arrangement makes the chopper design trivial, but the 1/7 filling factor in the 352.2 MHz sections leads to a mean bunch current of about 140 mA and hence to serious space charge problems not only in the SPL, but also at capture in the PS. However, this scheme can be considered as an option for the construction of the SPL in stages. In this case, the SPL would initially operate with Linac2 as injector at reduced current and with a longer beam pulse. Later on, the construction of a new 50 MeV injector would allow the full design current to be reached.

3 LINAC DESIGN

3.1 Low-Energy Room-Temperature Section

3.1.1 H^- Source

Probably the most important element in an accelerator chain is its source of particles. Whereas a source of positive particles is relatively easy to realise for high intensities, pulsed sources for negative ions have proved more difficult, although some very high powered dc devices have been developed for fusion research. In view of the number of different types available, the choice of a suitable source comes down to reliability and lifetime questions as long as the performance and characteristics are adequate. Magnetrons and Pennings generally have asymmetric emittance due to the slit geometry of the extraction. Multicusp converter and volume sources normally have symmetric emittances. There is also the question if the caesium, used in many sources to improve performance, could have medium to long term effects on the voltage holding of high field cavities and preinjector columns.

Laboratory	Type	*I* [mA]	Energy [kV]	ε^*_x	ε^*_y	Cs used	Reference	Notes
LANSCE	Surface	40	80			Y	[3.1]	12% duty [3.2]
Frankfurt	Multicusp	120	65	0.06		Y	[3.1]	Experimental ESS
Desy	Magnetron	35	18	0.28	0.25	Y	[3.2] p.199	
	RF volume	16	18	0.18	0.16	N		
		33	23			N		
JHP (KEK)	Volume	16	50	0.41		N	[3.2] p.293	90% Emittance
Grumman	Volume	10	40	0.1		N	[3.2] p.479	
JAERI	Volume	36	100	0.8		Y/N	[3.2] p.668	Multi-aperture
LAMPF	Surface	18	80	4		Y	[3.2] p.704	98% Emittance
NSNS	Volume	35	65	0.14			[3.2] p.749	Multicusp, objective
BNL	Magnetron	37	35				[3.2] p.779	
Efremov	Penning	15	20 (60)	0.21	0.11	N	[3.2] p.869	
		40		0.3	0.2	Y		
ISIS	Penning	35	665	2.1	3.0	Y	[3.3] p.1525	
LBL	RF	30	35	0.1		N	[3.3] p.1513	Multicusp
		100	19	~0.12		Y		
FNAL	Magnetron	50	750	1.6	1.8	Y	[3.4] p.917	90% Emittance
		65	750	1.8	2.6	Y		
LAMPF	Volume	18	80	0.2		Y	[3.4] p.1016	
Desy	RF volume	80	35			N	[3.5] p.992	Accelerated ?
NSNS	RF volume	35	30			N	[3.5] p.962	Achieved
Frankfurt	Volume	40	22			Y	[3.5] p.1012	ESS development

Table 3.1: Survey of H^- preinjector performances extracted from recent conferences (Linac98 [3.1], Linac96 [3.2], EPAC96 [3.3], PAC95 [3.4] and ICIS97 [3.5]). Emittances are μm, rms, normalised.

Table 3.1 is a compilation of H^- ion source performances derived from recent conferences and represents known, and in general demonstrated accelerator performance. Unlike protons, negative ion acceleration can be lossy. Transmission between source and linac can be as low as 34% with even further losses in the

linac [3.5]. The main cause of these losses is stripping of the H^- on the residual gas in the LEBT as negative sources often require high hydrogen pressures (a few 10^{-3} mbar in an open plasma chamber) which demands high capacity pumps and often pulsed gas supplies to maintain downstream pressures at a reasonable level. In a system designed to accelerate negative ions electrons will also be accelerated. Electron/ion ratios can reach 1000:1, but with careful design and optimisation this can probably be brought down to below 10:1. The dumping of these electrons at very low energy can give rise to aberrations in the ion beam and also contribute to stripping losses. Formation times for negative ions can, under certain conditions, be quite long (hundreds of microseconds) and measures might have to be taken to improve the rise time.

However with the present technology, it does not seem too difficult to meet the specifications of a negative ion source for the SPL provided that low energy losses can be kept under control or reduced. The main question would be which system to use. Arc discharge multicusp volume sources would seem, by their simplicity, to be a good choice, but their performance might be marginal unless caesium is added (which increases the complexity). The RF volume source looks good on performance but has the disadvantage of requiring much equipment at high voltage (or an RF isolation transformer). It is possible that, if the improvements carried out on the RF source [3.6] [3.7] were applied to a volume source, the specifications could be met, but this would require much more research and development which may not give the benefits desired. Both types of source given adequate cooling could meet an extended specification of 5% duty cycle. It will be of interest to follow the development of experimental multicusp source reported recently [3.8] to see if its performance can be transported to an operational accelerator.

3.1.2 Radio Frequency Quadrupoles

The first stage in the pre-injector chain of the SPL is a pair of RFQs in which the beam is accelerated to 7 MeV before injection into the DTL. Chopping of the beam has to be done before the DTL, and the preferred scheme is to do this between the two stages at 2 MeV.

The basic RFQ parameters are analysed below with their influence on the overall scheme and the criteria for the optimal choice.

The frequency is a very important parameter as it determines the focusing power and the length of the RFQ. The frequency must be equal to, or a sub-multiple of, the DTL frequency. The focusing parameter of the RFQ is proportional to the maximum field between the electrodes, the inverse of the square of the frequency and the inverse of the distance between the electrodes. Consequently, frequencies below 200 MHz are more suitable for very high current proton beams and higher frequencies (300-400 MHz) for low to moderate proton beams. Conversely, for successful chopping, lower frequencies are preferred as the chopper rise time should be shorter than the RF period. A frequency of 176 MHz (one half of the DTL frequency) has been chosen for the first RFQ and a frequency of 352 MHz for the second. The frequency jump between the RFQs requires particular attention to the longitudinal shaping of the bunch in the first RFQ.

The maximum field at the vane tip (and the maximum voltage between the electrodes) determines the length of the RFQ and the probability of breakdown. The Kilpatrick's criterion serves as a guideline: field values up to 2×Kilpatrick are common. To be conservative, the maximum field has been kept below 1.7×Kilpatrick.

The transition energy between the RFQs should not be too low to limit the effect of the debunching nor too high to limit the voltage needed in the chopper. The compromise value is 2 MeV.

As for more specific beam dynamics parameters, a special concern comes from the jump in frequency of a factor of two between the RFQs. This sets stringent requirements on the longitudinal emittance at the output of the RFQ1. The longitudinal emittance is formed in the first RFQ so that in this case it does not change after 2 MeV. This fact is exploited and the first RFQ designed with a very low voltage in order to form the longitudinal emittance as adiabatically as possible, while the second RFQ operates at higher voltage in order to keep the overall length within reasonable limits.

Both RFQs contain a dedicated matching section. The first RFQ has also been equipped with an output matching section to get a round beam with a radius of 8 mm at the chopper (100 % of the beam). The second RFQ, after a standard radial matcher, contains a rebunching section to make up for the elongation in the 1.6 m chopper line, corresponding to some 14 $\beta\lambda$ at 2 MeV and 176 MHz.

Table 3.2 summarises the main parameters of the proposed scheme. It should be stressed that these values are the result of a preliminary study and further optimisation is still possible.

	RFQ1	Chopper	RFQ2
Input energy	50 keV	2 MeV	2 MeV
Output energy	2 MeV	2 MeV	7 MeV
Frequency f_0	176 MHz		352 MHz
Voltage	140 kV	1.7 kV	100 kV
Maximum electric field	20 MV/m(1.4 K)		34 MV/m (1.7 K)
Length	2.3 m	1.3 m	4 m
Shunt impedance	100 kΩ m		80 kΩ m
Peak power	450 kW		500 kW
Average bore radius	8 mm		2 mm
Modulation factor (max)	2.0		2.5
Transmission (at 10mA current)	99%		100%
Design emittance (rms, norm)	0.2 μm		0.2 μm
Transverse acceptance (rms, normalised)	0.8 μm		0.6 μm
Output long. emitt. (rms, at f_0)	0.3 deg·MeV		0.6 deg·MeV

Table 3.2: Main Parameters of the RFQs.

3.1.3 Chopper

The structure considered for the SPL chopper is a pulsed electrostatic deflector based on the BNL design [3.9]. It comprises two deflecting plates segmented into strips which are perpendicular to the beam direction and which are connected by coaxial delay lines in order to match the deflecting pulse velocity and the beam velocity. As in the ESS design [3.10], the chopper is placed between two RFQs. The transfer energy of 2 MeV avoids the beam neutralisation problems of a chopper placed before the RFQ as well as the high voltage required by a chopper at high energy (between RFQ and DTL). The critical parameter is the chopper rise time. This needs to be shorter than the distance between bunches to avoid partially filled buckets, which could lead to losses at high energy. For the SPL, the frequency of the first RFQ is 176 MHz and the maximum phase length of the beam in the chopper is ±45°, which means that a rise time of 4.2 ns would be needed to avoid partially filled buckets.

An important feature of the SPL chopper is that transverse and longitudinal matching of the beam into the chopper and from the chopper into the following RFQ is achieved by matching sections inside the RFQs. This precludes the need for transfer lines and bunching cavities in front of the chopper. Between the RFQs there is a space of 1.6 m for the chopper and for some diagnostics, with a waist in the transverse and longitudinal planes at the chopper mid-position. The second RFQ includes a rebunching section and a standard radial matcher. In the present design, the effective chopper length is 1.3 m, the chopper voltage is 1.7 kV and the chopper aperture is 30 mm. The distance between the centre of the chopped and unchopped beams at the dump placed on the cover of the second RFQ is 30 mm.

3.1.4 Drift Tube Linac

The natural choice to cover the energy range between the RFQ (7 MeV) and the SC section (nominal input energy 100 MeV, with the option to go up to 150 MeV) is a Drift Tube Linac (DTL). RF frequency standardisation in the SPL and the higher shunt impedance make preferable a frequency of 352.2 MHz for the DTL, with respect to the first sub-harmonic (176.1 MHz). Moreover, the smaller cavity dimensions at that frequency allow a design with short tanks without quadrupoles inside the drift tubes. Bridge couplers can connect the tanks, and the focusing provided by quadrupole arrangements external to the tanks. This new approach has been already considered in many laboratories [3.11-3.15] for a wide range of duty cycles (0.2-100%). Of course, a more traditional DTL design based on long Alvarez tanks at 176 MHz or 352 MHz frequency with quadrupoles inside the drift tubes is possible for the whole energy range of the SPL DTL (7-150 MeV).

A traditional Alvarez-type DTL, due to the short focusing period ($2\beta\lambda$), is perfectly appropriate for low energy and/or high current beams and is unavoidable when the beam is strongly space charge dominated. On the other hand, a DTL with external focusing offers several practical advantages. First, the shunt impedance is higher because the drift tube design, without the constraint of housing a quadrupole, can be optimised for low capacitance. At 70 MeV the shunt impedance of an external-focusing structure at 352 MHz is 1.5 times higher with respect to an Alvarez structure at the same frequency [3.15]. Second, the mechanical construction of the tube becomes simpler, cooling is particularly easy and alignment of the drift tube is not critical. In particular, the drift tubes without quadrupoles inside have more relaxed

alignment tolerances, resulting in a less expensive tank construction. And finally, having direct access to the quadrupoles is particularly useful for re-alignment and repair. All these features make this kind of structure suitable for modern linacs, which use low current H^- beams, high RF frequencies and high energy RFQs.

In the case of the DTL for the SPL, space charge forces out of the second RFQ (7 MeV) are still high enough to require a short focusing period, making a structure with external focusing less attractive. For this reason, a single Alvarez DTL tank with FODO focusing, quadrupoles inside drift tubes and post-coupler stabilisation has been adopted in this study to accelerate the beam from 7 to 20 MeV. The transverse phase advance per period is set to 22° at peak current. Figure 3.1 shows the beam envelopes (x, y and energy) in this tank. The emittance blow-up is limited to 3% in the transverse and longitudinal planes.

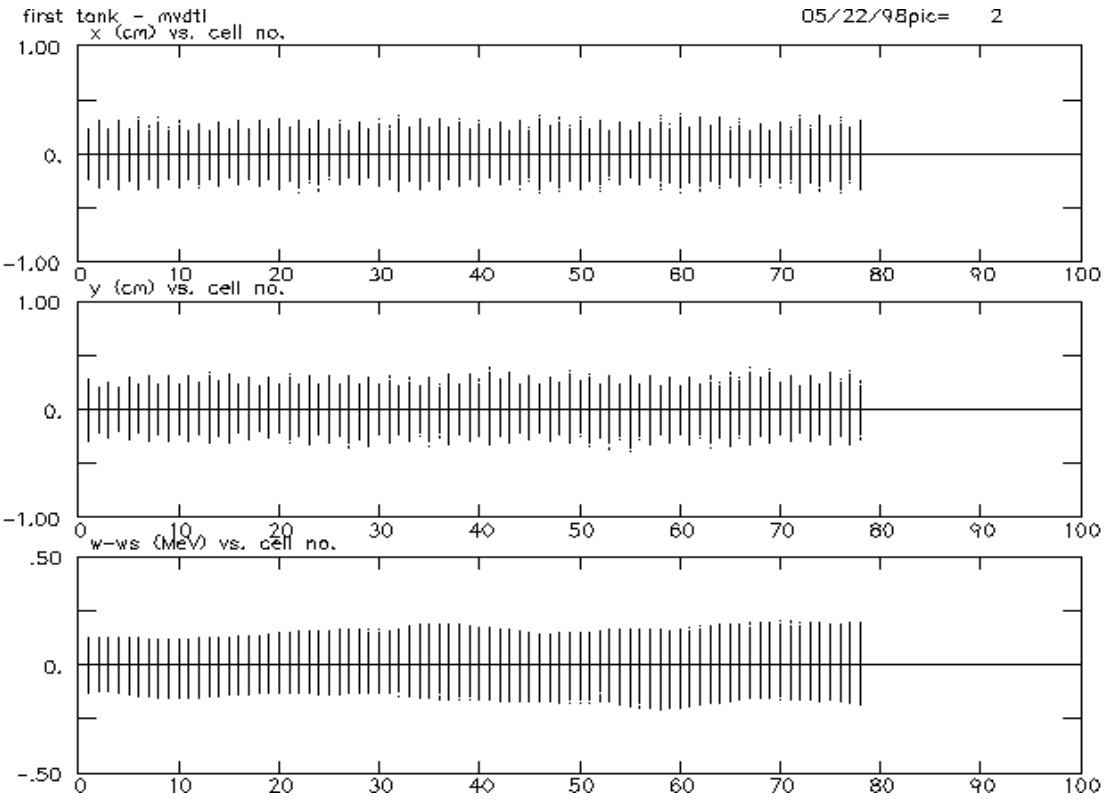

Figure 3.1: Beam envelopes in the first tank (standard Alvarez).

The main part of the DTL can be made of 8-cell tanks (each 8 $\beta\lambda$ long), separated by a 3 $\beta\lambda$ drift with a quadrupole triplet. A period is shown in Figure 3.2. Triplet focusing is preferred because of the resulting round beam inside the tanks, which minimises the emittance growth due to RF defocusing. The mean field in this section is 2 MV/m and the synchronous phase is -30°. The power distribution system, from the klystrons to the tanks, could be a branch system of the LEP type with one klystron feeding 8 or 4 tanks, or a more innovative layout with bridge couplers connecting the tanks and only one RF window per klystron.

Table 3.3 shows the main parameters of the proposed design. For convenience, it is divided into three sections (7-20 MeV, 20-104 MeV and the optional 104-150 MeV section).

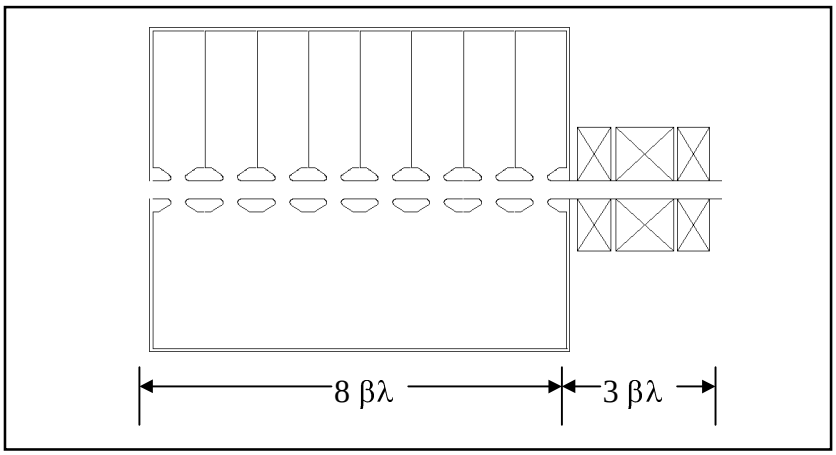

Figure 3.2: Basic DTL period (20-150 MeV).

		Section 1	Section 2	Section 3	
Input energy	W_{in}	7	20	104	MeV
Output energy	W_{out}	20	104	150	MeV
Type of structure		standard Alvarez	external quads	external quads	
Frequency	f	352.2	352.2	352.2	MHz
Mean field	E_0	2	2	2	MV/m
Number of cells per tank	n	78	8	8	
Number of tanks	N	1	28	12	
Tank diameter	D	0.54	0.52-0.49	0.47	m
Tank length	l	10.8	1.41-2.94	2.98-3.42	m
Bore diameter	d_b	24	30 - 36	36	mm
Drift tube diameter	D_t	160	80 - 100	100	mm
Synchronous phase	ϕ_s	-30	-30	-30	deg
Shunt impedance	ZT^2	20 - 27	70 - 39	39 - 28	MΩ/m
Peak surface field	E_p	7.5	17	18	MV/m
Length	L	10.8	87.6	55.2	m
Peak power	P_{tot}	1.1	4.7	3.3	MW
Number of klystrons	N_k	1	5	3	
Number of tanks per klystron		1	8 - 4	4	
Focusing		FODO	triplets	triplets	

Table 3.3: Main DTL Parameters.

For the analysis of the sections with external focusing, the code PARMILA [3.16] has been used in conjunction with a routine specially written to analyse strings of tanks with external focusing [3.15]. The matching of the sections between 20 and 150 MeV is not yet optimised, as can be seen in Figure 3.3, which shows the beam rms radius at tank centre as a function of beam energy. Mismatch is apparently the origin of the 10% transverse emittance growth, which occurs mainly at high energy, while emittance growth in the longitudinal plane is negligible (Figure 3.4). At

20 MeV, the transverse phase advance per period at zero current is 105° and the tune depression is 0.8. The transverse emittance assumed in the simulations is 0.35 μm.

Further studies will focus on extending the structure with external quadrupoles towards a lower energy by reducing the number of cells per tank and on optimising the focusing. What is considered as the main limitation of the present preliminary design is the sharp change of focusing period from the Alvarez tank to the external focusing DTL. A better optimised design should split this jump into smaller changes in focusing period that would finally allow a gradual transition from the short RFQ focusing period ($\beta\lambda$) to the long period imposed by the cryostats to the SC part ($10\beta\lambda$). Particular effort has to be made to achieve good matching between the different sections in order to avoid emittance growth and halo formation.

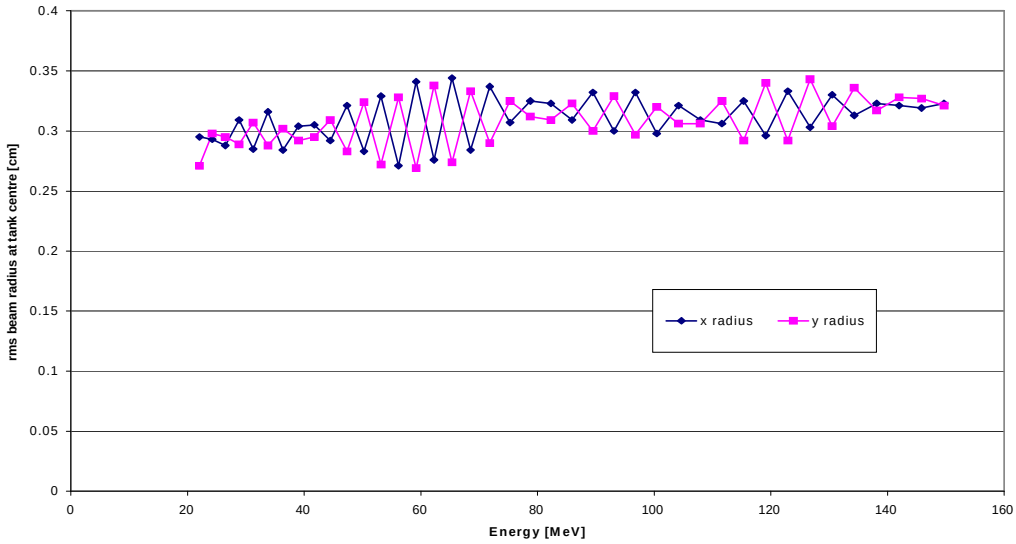

Figure 3.3: Rms beam radius at tank centre along the DTL (20-150 MeV).

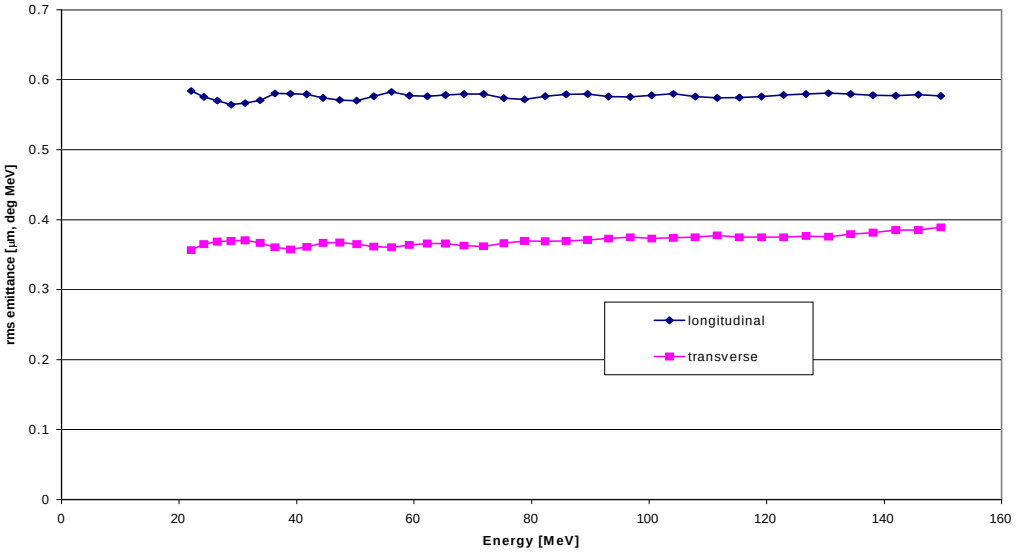

Figure 3.4: Rms emittances along the DTL (20-150 MeV).

3.2 High-Energy Superconducting Section

3.2.1 Basic Choices and Overall Layout

The SC part (SCL) of the SPL comprises four different sections made of 352.2 MHz superconducting cavities optimised for beta of 0.48, 0.625, 0.8 and 1 respectively. Standard LEP-2 4-cell cavities designed for particles with β=1 (Figure 3.5) are used at energies above 1 GeV. The basic cells for the "reduced-beta" cavities are shown in Figure 3.6. They are arranged in 4-cell cavities (β=0.48, 0.625) and 5-cell cavities (β=0.8) [3.17]. Figure 3.7 shows the transit time factor, *T*, as a function of beam energy for the four basic cavities composing the sections.

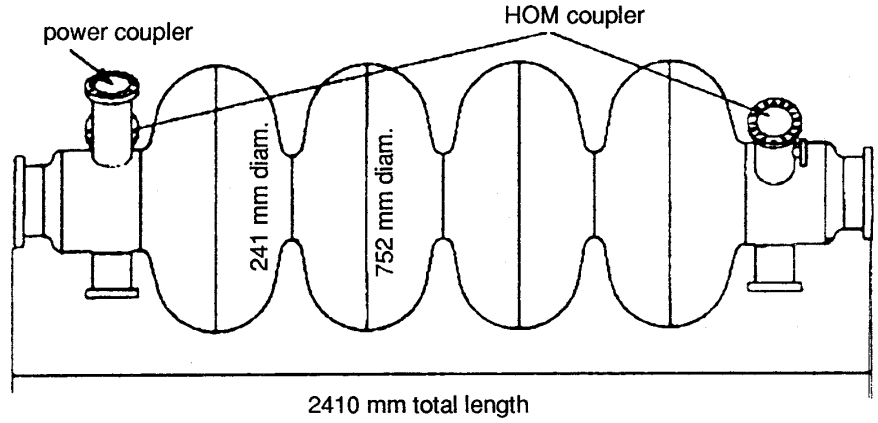

Figure 3.5: Basic LEP-2 cavity.

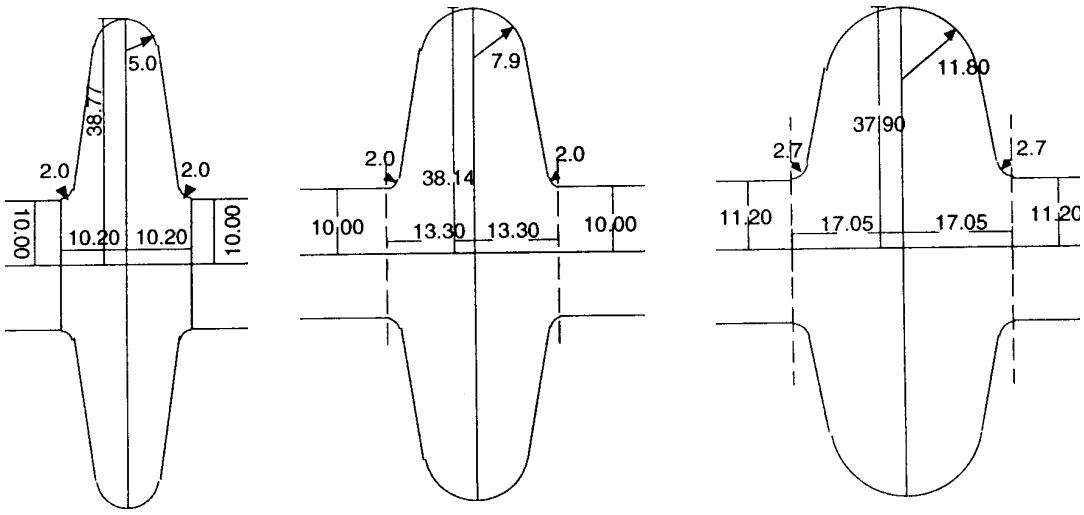

β=0.48 β=0.625 β=0.8

Figure 3.6: Shape of "reduced-beta" SC cells (dimensions in cm, from [3.17]).

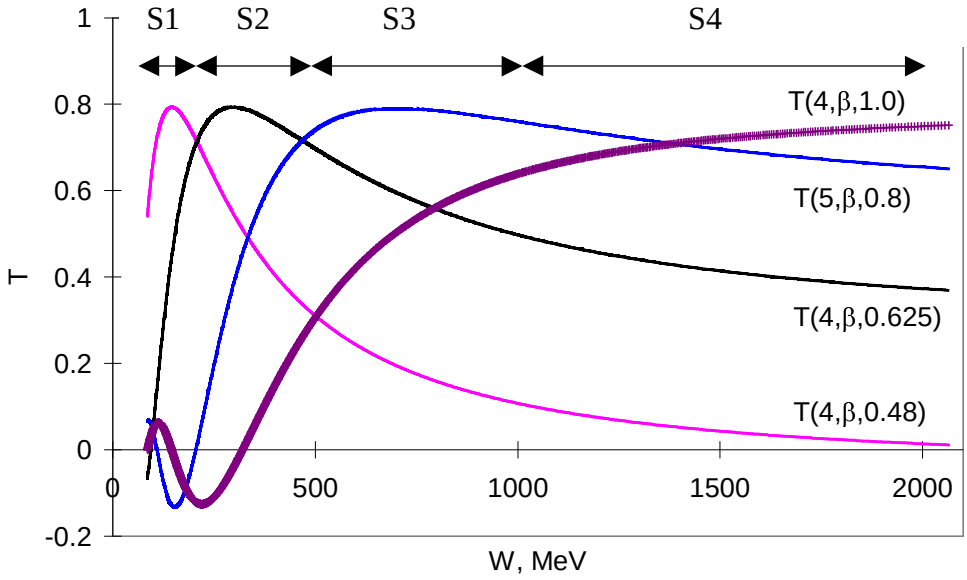

Figure 3.7: Transit time factor, T(N, β, β_g), as a function of energy, W, for the four sections of the SCL.

The transit time factor takes into account the reduction in acceleration efficiency due to phase slip when a cavity of N cells optimised for a geometrical beta β_g (i.e., made of cells $\beta_g\lambda/2$ long) is used for particles of relativistic velocity β. The curves in Figure 3.7 have been obtained by an analytic calculation based on a sinusoidal approximation to the real field distribution on axis calculated by the program Superfish [3.18]. The resulting transit time factor is a function of N, β and β_g.

The efficiency of the existing LEP-2 cavities, which were built for $\beta_g = 1$, goes down rapidly with decreasing energy. While it would be feasible to use them for protons above about 500 MeV ($T \approx 0.3$), a more efficient solution considered here is to build new 5-cell cavities optimised for $\beta_g = 0.8$ and install these in the existing LEP-2 cryostats [3.19]. This arrangement covers the energy range efficiently between 500 MeV and 1 GeV, as can be seen in Figure 3.7. Two additional sections of 4-cell cavities optimised for $\beta_g = 0.48$ and $\beta_g = 0.625$ installed in shorter cryostats cover the energy range efficiently between 100 MeV and 200 MeV and between 200 and 500 MeV, respectively. The cryostat and cavity arrangements in the four sections are shown in Figure 3.8.

The composition of the SCL, from 100 MeV to 2 GeV, is given in Table 3.4. The overall length takes into account a distance of $3\beta\lambda$ between cryostats for doublet focusing. Each cryostat contains four cavities and eight cavities are fed by the same klystron. From the power point of view, the first 5 klystrons (up to 350 MeV) can feed 16 cavities each, but this solution leads to a lower energy stability at the end of the SCL due to the reduced feedback loop efficiency and is discarded for the moment, until more data are available. The alternative lower number of klystrons is indicated in parenthesis in Table 3.4. For a total power of 19 MW, 36 klystrons of 1 MW output power are installed, leaving a large margin for amplitude and phase control and for a possible upgrade of the linac current. Details of the mean field and synchronous phase corresponding to this layout are given in Section 3.2.3.

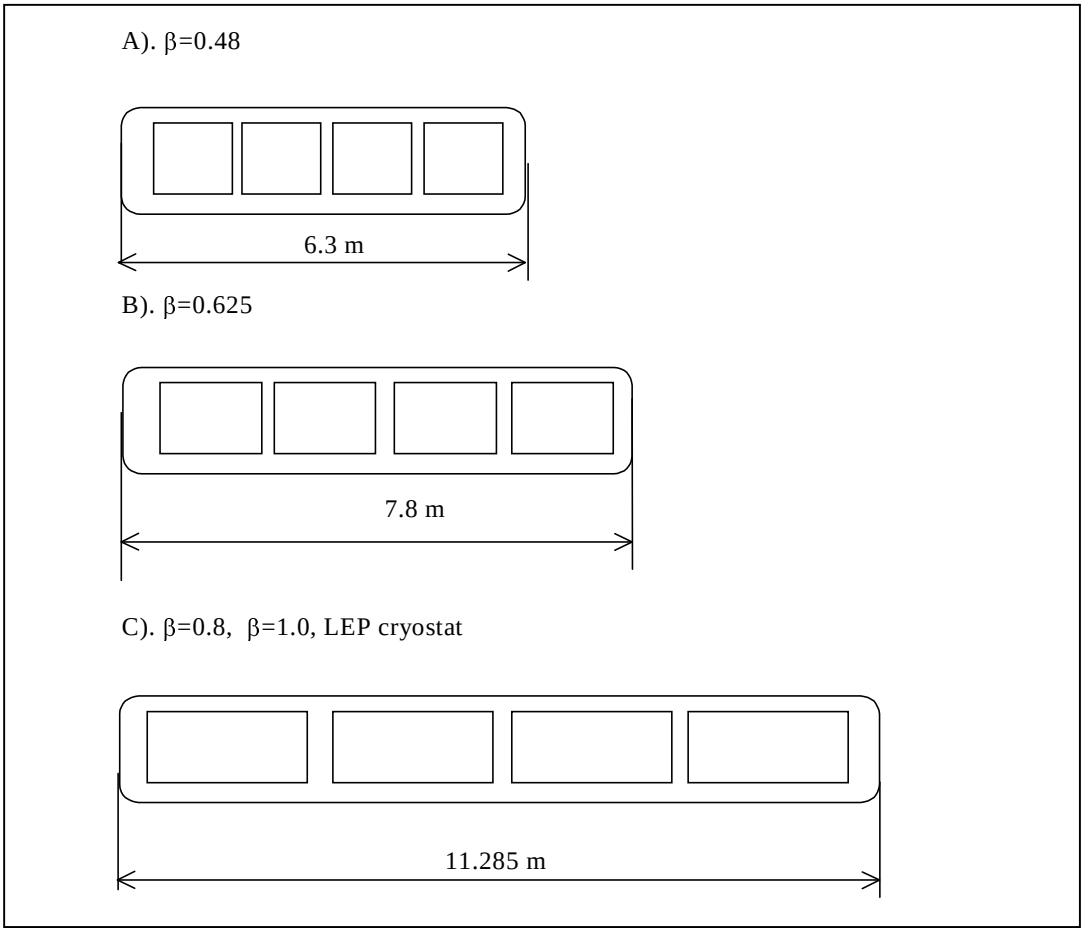

Figure 3.8: Cavity and cryostat layout in the four SC sections.

Sec.	β_g	No Cryostats	No Klystrons	No Cavities	No Cells per Cavity	Output Energy [MeV]	Length [m]	RF Power [MW]
1	0.48	8	4 (2)	32	4	191	58	0.9
2	0.625	14	7 (4)	56	4	452	126	2.6
3	0.8	16	8	64	5	1027	188	5.8
4	1.0	34	17	136	4	2041	407	10.1
Tot.		72	36 (31)	288			779	19.4

Table 3.4: Composition of the SCL.

This scheme re-uses 34 LEP-2 4-cavity modules with their cryostats, i.e. 53% of the 68 installed in LEP. Moreover, 16 cryostats are employed for the $\beta_g = 0.8$ cavities, giving a total of 52 cryostats re-used (76%). Depending from the amount and the status of the available equipment, an energy exceeding 2 GeV could be achieved by using the rest of the cavities.

The option of using LEP-2 cryostats for all the SCL has been analysed. In this case, 6-cell cavities for $\beta_g = 0.48$ and $\beta_g = 0.625$ would be installed in the existing

cryostats, but the longer focusing period at low energy drastically limits the maximum current.

The optimisation of the transition energy between the RT and SC sections requires a cost analysis that goes beyond the purpose of this study. The SC cavities at the lowest β will probably be made out of bulk niobium, while the high-energy part of the DTL, although less expensive, is inefficient from the power point of view. The optimum transfer energy will be the result of a careful cost optimisation, possible only when all the parameters involved are known. For the moment, it is assumed that the transition is at 100 MeV. If a transfer energy of 150 MeV or higher is chosen, the entire section with $\beta_g = 0.48$ cavities can be discarded and the $\beta_g = 0.625$ section extended to lower energy.

Phase adjustment between cavities is obtained by matching the space between cavities inside and outside the cryostats to the particle velocity. However, for the existing LEP-2 modules the distance between cavities inside the cryostats is fixed, meaning that high power phase shifters are needed to adjust the individual cavity phases.

A precise strategy has to be elaborated for tuning up such a linac, i.e., for finding the correct klystron amplitudes and phases during the running in and after a shutdown. Below 500 MeV, the "Δt procedure" can be used. In this technique, comparing the beam phase in two pick-ups with one module switched on and off makes a relative energy measurement. At higher energies, the increase in particle velocity per module is small and this technique becomes unreliable. Above 500 MeV, it should be possible to use the "phase scan signature" technique. This involves scanning the complete 360° phase settings of a module, producing a large change in energy that is easier to measure. Calculations show that the size of the energy change depends only slightly on the input energy. This prevents errors in the setting from becoming larger and larger along the linac.

Pulsed operation of the SC cavities will be required to minimise heat dissipation in the structures and average power consumption. For a loaded Q-value of 2.6×10^6 (LEP-2 cavities) the beam is injected after 1.62 ms. The corresponding form of the voltage pulse in the cavities is shown in Figure 3.9 for two cases, corresponding to the nominal pulse length of 250 μs (LHC beam) and to a pulse length of 1 ms that can be used for other applications.

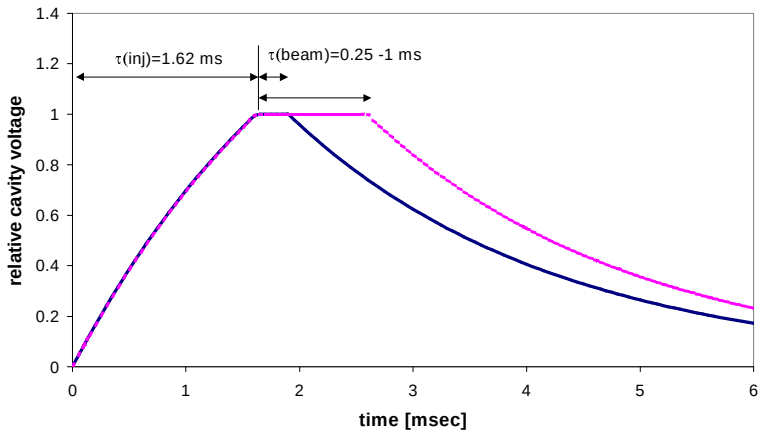

Figure 3.9 : Voltage pulse on the SC cavities.

Microphonic and radiation pressure effects due to the pulsed operation of the SC cavities can be compensated by stabilising loops (Section 3.2.4). At the duty cycle considered (≤ 5%), static cryogenic losses will dominate. Taking a static loss of 180 W per 4-cavity module (Section 3.4), the overall cryogenic power loss for the 72 cryostats of the SCL is 13 kW, about the cooling capacity of a LEP-type cryoplant. LEP is presently equipped with four cryoplants, but these cannot be recuperated because they will be re-used for the LHC. Applying the LEP-2 conversion factor of 225 W/W, the electrical power needed for refrigeration would be about 3 MW.

An important option that can be exploited for the SC section is to run the LEP-2 cavities at a field higher than 6 MV/m. This is possible because pulsed operation reduces the probability of quenching and because only about 50% of the LEP-2 cavities will be recuperated, allowing only those with the highest gradient to be selected. Finally, reductions in the *Q*-value at high field can be tolerated because the RF cryogenic losses are negligible compared to static losses. However, these performances must be confirmed experimentally and, for this reason, the present study is based on the conservative assumption of a 6 MV/m field.

3.2.2 Reduced-beta Cavity Development

The availability of a large SC RF system after LEP decommissioning has prompted the study of SC cavities with β less than unity (typically $0.5 < \beta < 1$) in order to extend the possibilities of re-using LEP equipment in a proton linac. The technology developed at CERN for the LEP-2 project seems rather attractive for such an application for several reasons.

- The low frequency chosen for LEP allows a large iris aperture (200 - 240 mm) and a greatly reduced probability of beam losses along the accelerating structure.
- The niobium-on-copper technology has a number of advantages: no magnetic shielding is necessary, no hard quenches are observed, the material cost is greatly reduced - in particular for low-frequency cavities - and, finally, little cost increase occurs if the structure needs to be strengthened against mechanical instabilities. This is especially true for reduced-beta cavities with almost flat side walls.

Consequently, in 1997, CERN launched a test programme to evaluate the feasibility of reduced-beta cavities using LEP-2 technology, the first results of which were presented that same year at the 8th Workshop on RF Superconductivity [3.17]. The main outcome of this study (which is still in progress) is summarised below.

Scaling from a $\beta = 1$ cavity to a lower β means reducing proportionally the length of each cell whilst keeping the equator diameter more or less constant (at constant frequency). In doing so, the geometry factor becomes less favourable (there is more stored energy for the same accelerating voltage and more wall losses for the same stored energy). Even with the same quality of niobium layer, the performance would not be as good as that of standard $\beta = 1$ cavities.

Single cells with three geometries ($\beta = 0.48$, $\beta = 0.625$ and $\beta = 0.8$) have been constructed and tested at liquid helium temperature. There was no sign of multi-pactoring, nor were any quenches recorded. However, a decrease of the quality factor was observed. This decrease was much larger than that calculated and became more pronounced for lower β cavities. The most convincing explanation lies in the

influence of the angle of incidence of the niobium atoms when the SC layer is deposited. The shorter the cavity (for lower β), the smaller the average angle of incidence. To counter this effect, a shorter magnet will be used to localise the magnetron discharge more precisely during deposition. In addition, specific tests with samples coated at different incidence angles have been undertaken. The first aim is to investigate the effect on surface structure (existence or not of a column structure) and, later, the RF properties of such samples will be measured with a quadrupole resonator [3.20, 3.21].

The single-cell $\beta = 0.8$ cavity has RF properties which were considered acceptable and, therefore, it was decided that a five-cell $\beta = 0.8$ cavity could be built using LEP technology. Such a cavity could fit directly into a LEP cryostat (which normally houses four $\beta = 1$ cells), thus re-using all ancillary equipment including tuner bars, couplers, HOMs, cryogenic circuits and also the so-called cavity "cut-offs", i.e. the beam tubes with their various flanges, which represent more than half the cost of a multicell cavity.

3.2.3 Beam Dynamics

The beam dynamics through the SCL has been computed with the program LANA [3.22], which generates a distribution of particles in 6-D phase space and integrates the motion in a field distribution generated by the cavity design code Superfish [3.18]. Space charge effects are taken into account.

The starting distribution was 6-D waterbag with rms normalised emittance of 0.4 μm and rms longitudinal emittance of 0.6 π deg MeV. These values result from the general emittance budget discussed in Section 2 and given in Table 2.1b and 2.1c.

The SCL has been first of all optimised for zero current. In this case, the phase advance per focusing period is 80°. Figures 3.10-3.12 show the evolution of the beam transverse envelopes, of the phase and of the energy spread along the SCL. A small mismatch in the transverse plane is generated at the transition between the different type of cryostats. Finer local optimisation of the quadrupole fields should take care of this. In the longitudinal plane, the matching is not perfect due to the sharp change of the effective accelerating gradient at the transition between the sections of different β (see Figure 3.13). The effect of the mismatch is very small for zero current: only a residual oscillation of the longitudinal envelope of some 0.1° results at the end of the SPL. However, for the nominal current further work is necessary to improve both transverse and longitudinal matching since, in the presence of space charge, such mismatches can cause emittance growth in the three planes.

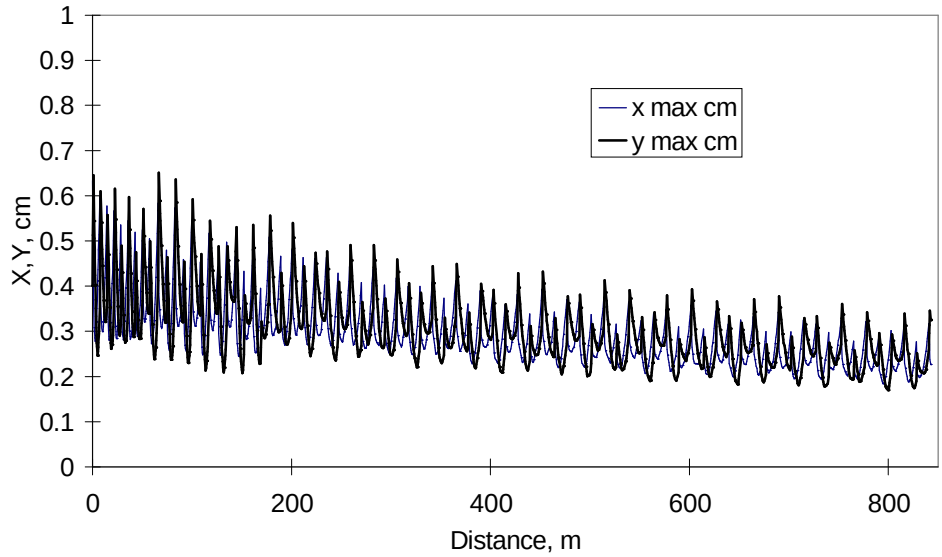

Figure 3.10: Transverse envelopes (all particles) along the SCL for zero current.

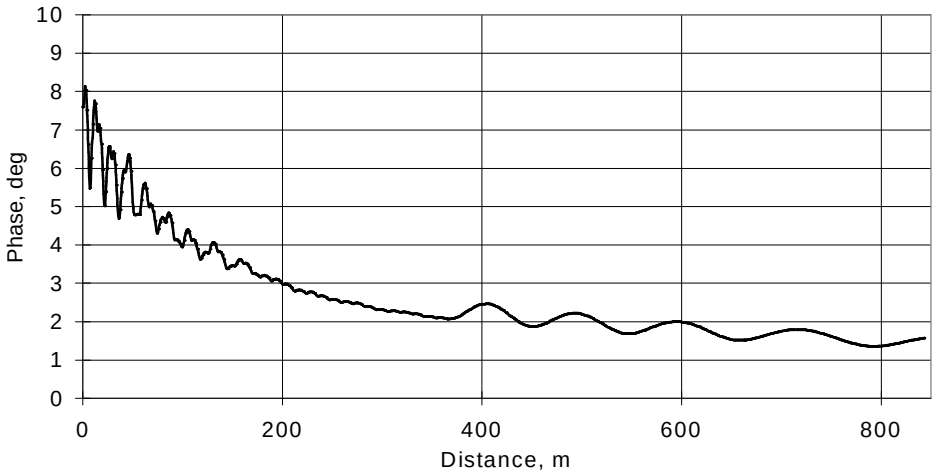

Figure 3.11: Half width phase spread, $\sqrt{5}\ \varphi_{rms}$, along the SCL for zero current.

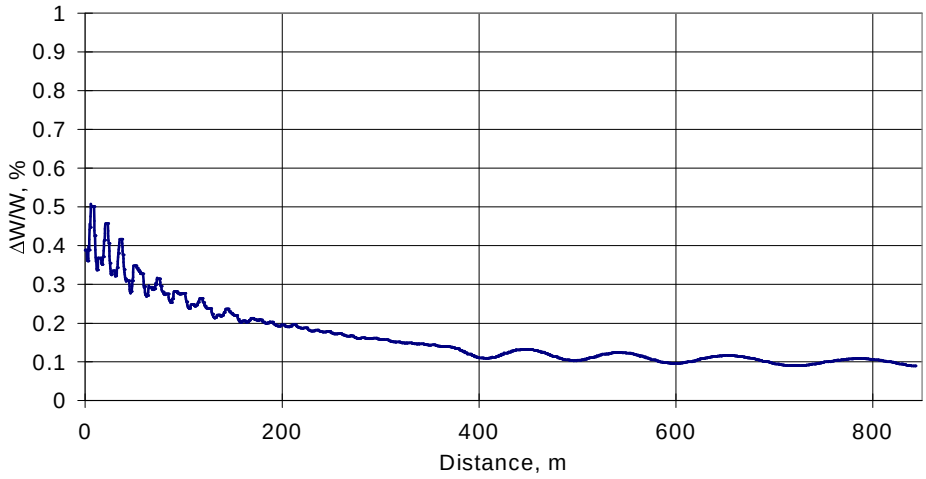

Figure 3.12: Half width relative energy spread, $\sqrt{5}\ (\Delta W/W)_{rms}$, along the SCL for zero current.

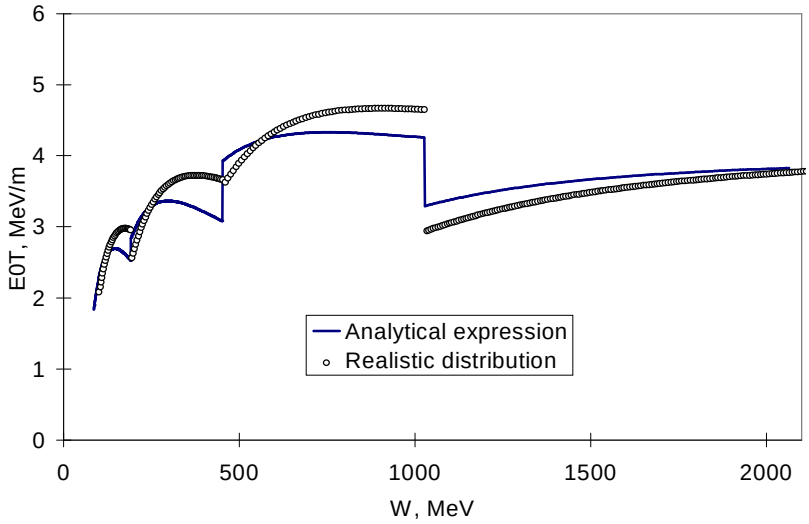

Figure 3.13: Effective accelerating field vs. energy (LANA integration of SUPERFISH data).

The longitudinal acceptance of the SCL has been calculated by populating a large area in the input phase plane, tracking each particle through the machine and then following back the particles accepted. This takes into account the effect of the stray fields at the edges of cavities, which cannot be neglected in this case. The phase space plot of the accepted particles is shown in Figure 3.14.

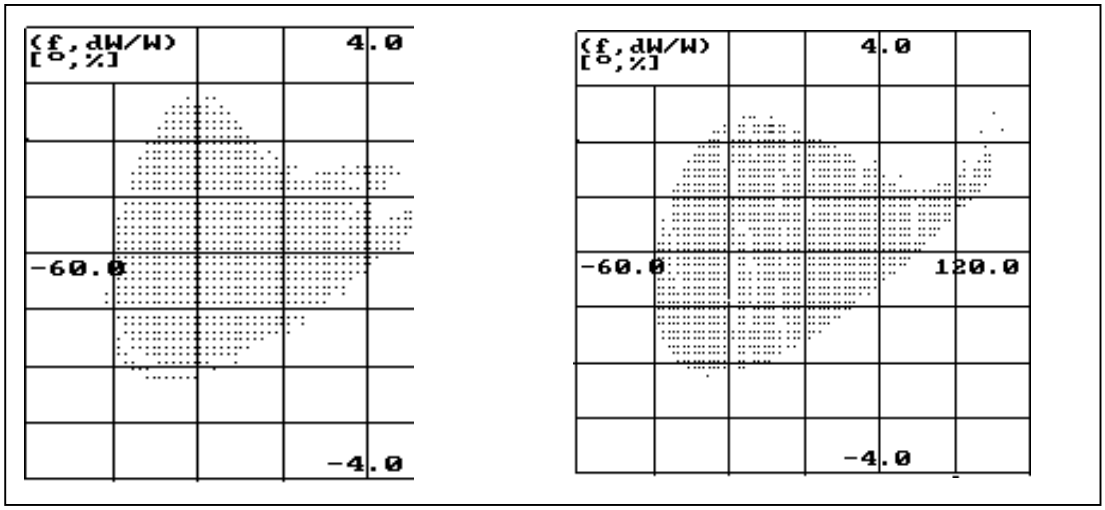

Figure 3.14: Longitudinal acceptance at 100 MeV and at 191 MeV (end of the β=0.48 section).

For the zero-current case, a preliminary study of the sensitivity of the output beam quality to RF field errors has been performed. Random phase and amplitude errors have been generated uniformly in a given range and used in 400 beam dynamics runs. The errors assumed here are residual random errors that can be expected after the action of the feedback systems (Section 3.2.4).

In Figure 3.15, the energy spread of the bunch and its energy deviation along the SCL are shown for phase errors within ±3° and amplitude errors within ±3%. Figure 3.16 shows these parameters for phase errors within ±10°. The energy acceptance along the SCL is also shown for comparison.

In all cases, there is no instantaneous emittance growth in either longitudinal or transverse planes. In principle, phase errors up to ±10° are still acceptable in the SCL as the bunch still stays inside the acceptance, but the large energy deviation produced at the SCL output (about 20 MeV) is larger than the PS energy acceptance and has to be reduced by an energy-correcting cavity placed at the end of the transfer line to the PS.

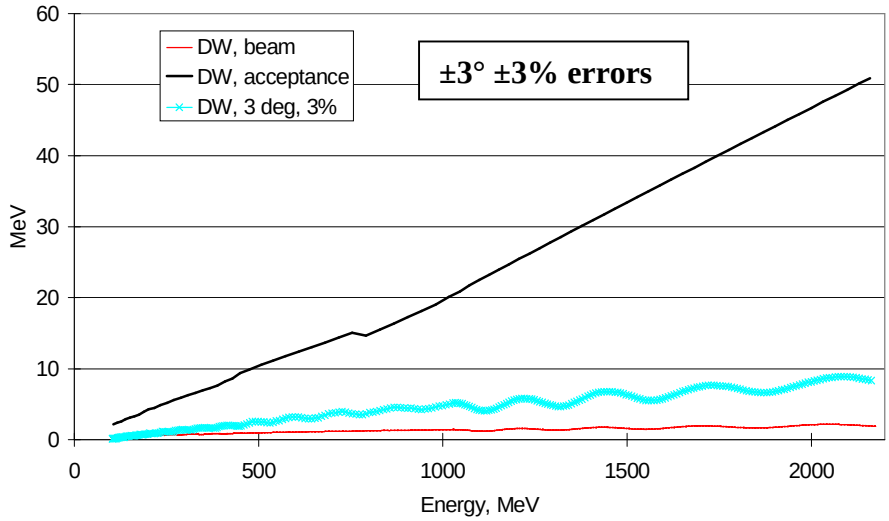

Figure 3.15: Half width energy spread, $\sqrt{5}\,\Delta W_{rms}$, along the SCL. From bottom to top: energy spread inside the bunch; bunch centre deviation for ±3°, ±3% random cavity errors; and energy acceptance from analytical calculations.

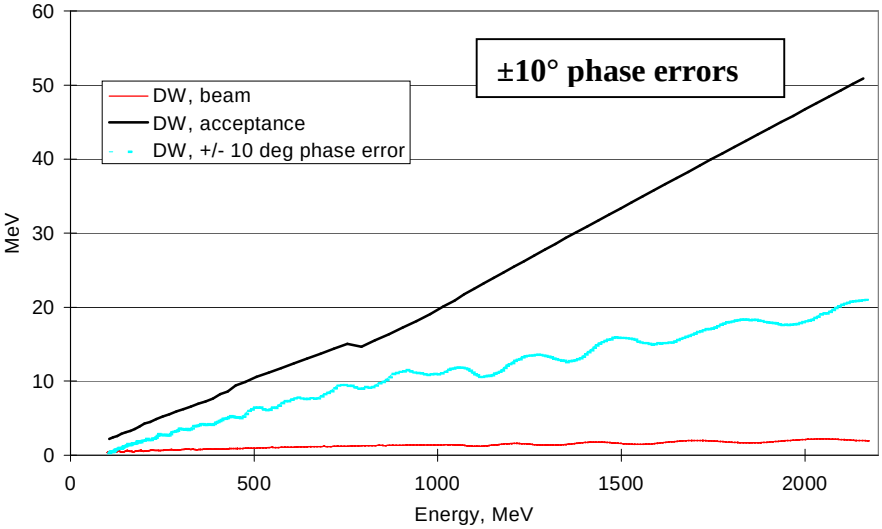

Figure 3.16: Half width energy spread, $\sqrt{5}\,\Delta W_{rms}$, along the SCL. From bottom to top: energy spread inside the bunch; bunch centre deviation for ±10° random cavity phase errors; and energy acceptance from analytical calculations.

Some preliminary simulations with space charge (40 mA current) show a transverse rms emittance growth and a decrease of the longitudinal rms emittance. This seems to indicate a redistribution of energy between the longitudinal and transverse phase planes (equipartitioning) due to coupling between the planes through space charge forces. The relative emittance growths along the SPL in the 3 planes are shown in Figure 3.17. The 45% transverse emittance growth is due to the action of space charge on the largely asymmetric bunch and to the transverse mismatch between the cryostats of different types.

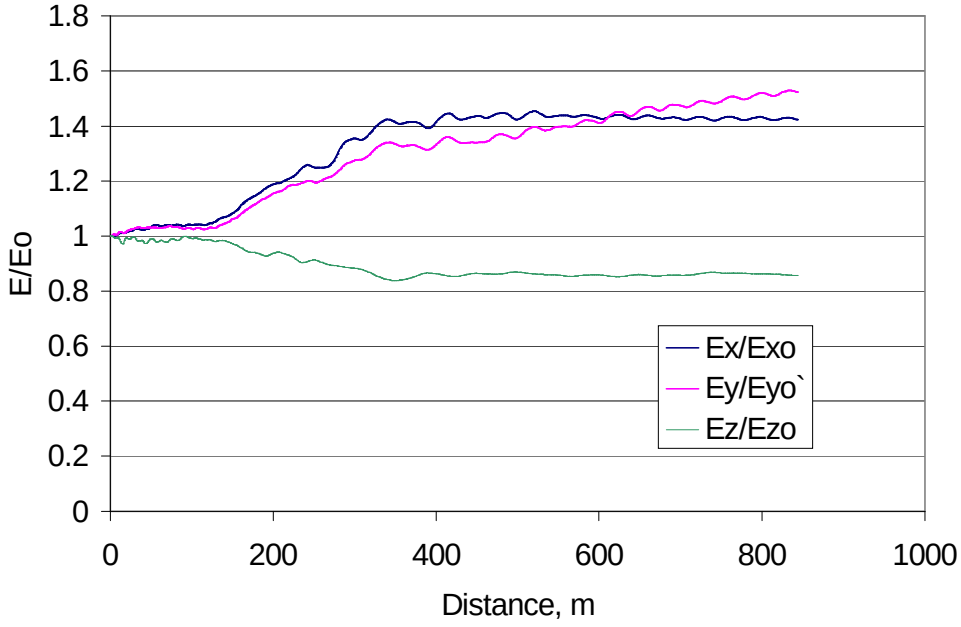

Figure 3.17: Relative rms emittance growth along the SCL, I=40 mA.

In order to reduce the emittance growth by improving the equipartitioning of the beam emittances it is necessary to provide stronger focusing in the transverse plane or weaker focusing in the longitudinal plane below 1 GeV. While the latter would result in the loss of the main advantage of a superconducting linac, a stronger focusing can be more easily applied, either by shortening the cryostats in the reduced-beta sections or by placing superconducting quadrupoles inside the cryostats. Already in the present design there is some margin for reducing the distances between cryostats at low energy, where shorter quadrupoles can be used. A reduction of mean bunch current would also reduce considerably the emittance growth. For example, a mean bunch current of 20 mA, which could be obtained by a more sophisticated chopping system filling all the buckets, has been tried in the simulations, resulting in 28% emittance growth.

Above 1 GeV the LEP cryostats can be used, because as it follows from Figure 3.17 after an energy of about 900 MeV the equipartitioning factor is about unity and the emittances are stable.

3.2.4 Beam Energy Stability

Microphonic vibrations of the SC cavities are considered as the main source of field (amplitude and phase) errors in a pulsed SC linac and are treated specifically in this Section, together with a correction scheme based on RF feedback of the cavity voltage and phase.

Vibrations of the SC cavities at their mechanical resonance frequencies (typically, some tens of Hz) can be excited either by the cavity environment, in particular by turbulences of the coolant, or by the strong Lorentz forces acting on the cavity walls during the RF pulse. Small vibration amplitudes and the corresponding small cavity detuning can in high-*Q* SC cavities induce large voltage drops and phase shifts. The effect on the beam of such voltage and phase errors is to excite synchrotron oscillations of the beam centre that can lead to beam losses in the linac or in the PS, if the linac beam falls outside the PS longitudinal acceptance.

To reduce the effect of the cavity vibrations RF feedback of the cavity voltage and phase can be applied at the klystron input. For the SPL, a feedback scheme and calculation tools developed for electrons in the frame of the TESLA project [3.23] have been adapted to the non-relativistic proton beam. The principle of the self-excited loop used in both cases is shown in Figure 3.18. The frequency of the loop tracks the cavity frequency in order to stabilise the amplitude of the cavity voltage. To reduce the amplitude and phase fluctuations of the cavity voltage during the beam pulse, two signals are injected respectively in phase and in quadrature in the self-excited loop to modify the voltage of the generator proportionally to the detected amplitude and phase errors.

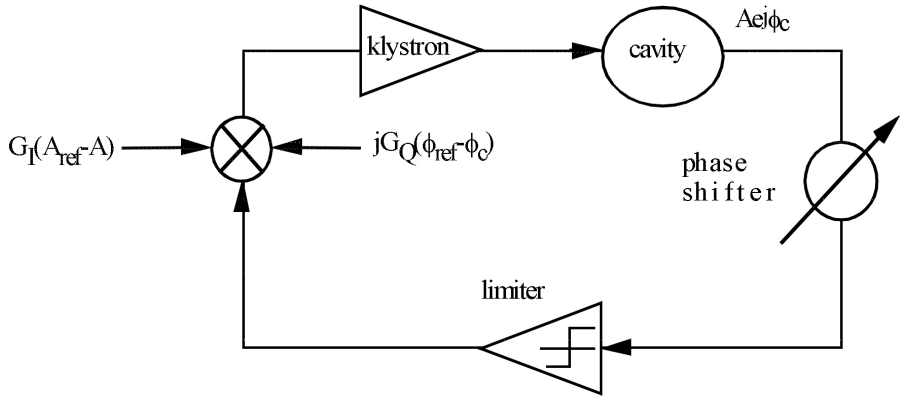

Figure 3.18: Cavity inserted in a self-excited loop with two signals injected in phase (regulation of amplitude) and in quadrature (regulation of phase). A_{ref} and ϕ_{ref} are the amplitude and phase references. G_I and G_Q are the gains of the amplitude and phase loops.

The RF loops can stabilise the cavity voltage and phase only partially when a klystron feeds a string of cavities, all independently vibrating. In the case of the SPL the feedback loop tracks the average frequency of the eight cavities connected to each klystron and takes the vector sum of the eight voltages, leaving a residual error with an effect on the beam. For a given random error distribution in the 288 cavities of the SCL, the code used in the simulations calculates the motion of the beam centre and the residual energy and phase errors at the exit of the linac for the individual bunches

inside the pulse, taking into account the action of the feedback loops. The code assumes that the frequency of the cavities does not change during the RF pulse, because the period of the mechanical vibrations is much larger than the beam pulse duration of 500 μs taken in the computations. The simulations take into account as well the detuning due to Lorentz forces, which is compensated by the feedback loop. For the calculation of the Lorentz force effect, the detuning parameter, 2 Hz/(MV/m)^2, and the mechanical response time, 10 ms, of the LEP-2 cavities have been assumed for all the linac.

In the absence of precise measurements of the amplitude of microphonic vibrations in the LEP-2 cavities in pulsed mode, two test values have been taken as maximum frequency error in the simulations, ±20 Hz and ±40 Hz. These two cases correspond to large phase errors of ±13° and ±24°, respectively, and are considered as very conservative. The present experience with pulsing LEP-2 cavities (during conditioning, for example) does not indicate excessive vibration levels.

The simulation program takes a uniform distribution of cavity errors between the two limit values. Without the feedback loops, the beam is lost in the linac in both cases. With the feedback loops and the gain set to 100 for both loops, the beam is transported to the end of the linac. The effect of the Lorentz force is small at the relatively low accelerating gradient of 6 MV/m and is constant from pulse to pulse. The phase loop can be easily set as to compensate for it, and its effect on the beam can be neglected in comparison to the effect of vibrations.

The results of the analysis of 500 error distributions are summarised in Table 3.5. For each distribution, the program computes the energy and phase errors at 2 GeV for all bunches inside a 500 μs beam pulse. The table reports the rms value of the relative energy error inside the single beam pulses, and the rms value of the relative energy error for the 500 cases. The latter represents the energy error of different beam pulses, for which the errors are not correlated. The energy variation inside the pulse is very low, coming essentially from the finite bandwidth of the feedback loops, while the energy jitter between different pulses is more than one order of magnitude larger. Figure 3.19 shows the position of the bunch centre (averaged inside the single pulses) relative to the synchronous particle for the 500 pulses. The rms energy offset at 2 GeV is 3.1 MeV for ±20 Hz vibrations and 5.8 MeV for the ±40 Hz case. The additional RF power required by the feedback loops is also given in the Table.

Maximum vibration detuning	±20 Hz	±40 Hz
$(\Delta W/W)_{rms}$, inside pulse	4.05×10^{-5}	1.52×10^{-4}
$(\Delta W/W)_{rms,}$ pulse-to-pulse	1.53×10^{-3}	2.92×10^{-3}
Additional RF Power, worst case	5%	15%
Additional RF Power, average	2%	5%

Table 3.5: Energy spread at 2 GeV and additional RF power for two vibration amplitudes.

The longitudinal rms beam emittance at 2 GeV, 0.6 π·deg·MeV, is much smaller than the overall surface occupied by the beam in the longitudinal plane in presence of errors (Figure 3.19). It is therefore possible to consider this surface as an overall longitudinal beam emittance in presence of vibration errors. The value of the overall rms emittance for the two cases of Figure 3.20 is 6 π·deg·MeV for ±20 Hz errors and 25 π·deg·MeV for ±40 Hz errors.

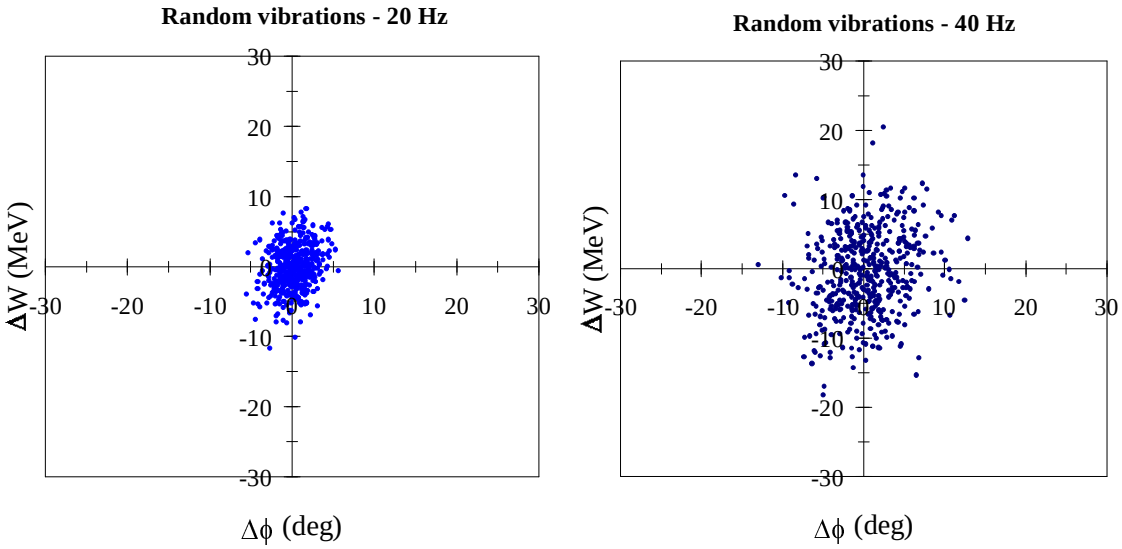

Figure 3.19: Average energy vs. average phase inside a pulse at 2 GeV for 500 different pulses and two vibration amplitudes.

3.3 Debunching Cavity and Transfer Line to the PS

A transfer line and a debunching cavity acting as an energy corrector are required between the SPL and the PS to compensate part of the energy jitter induced by microphonic vibrations in the SC cavities. Calculations have been made with TRACE3D [3.24] assuming an overall phase and energy spread at 2 GeV of ±7° and ±10 MeV, respectively. The values given in this Section for energy and phase spread are total ones in the TRACE convention, i.e., ±√5 rms. This emittance contains 99.8% of the cases computed in Section 3.2.4 for vibration amplitude of ±20 Hz and 76% of the cases for ±40 Hz vibrations. The energy acceptance of the PS being about ±2 MeV, an RF cavity is necessary to correct for the overall energy spread.

The length of the line is dictated by the longitudinal dynamics, as it is necessary to let the beam overall emittance spread out in phase before the RF cavity can reduce the energy spread. The 352.2 MHz cavity (which can be another LEP-2 standard module) is placed 200 m downstream from the exit of the SPL, where the overall phase spread is ±35°. The effective voltage required is then 16 MV, to get an output energy spread (i.e., residual jitter of the mean beam energy from pulse to pulse) of ±2 MeV.

As for the transverse plane, the line comprises four focusing periods each 52 m in length and each with a phase advance of 140°. This limits the dimension of the beam to 15 mm in the worst case. Figure 3.20 shows the initial and final transverse

(top) and longitudinal (bottom) emittance and the beam envelopes from the output of the SPL to injection in the PS. There is sufficient space in the line for the bending elements that would be needed, depending on the relative position of SPL and PS on the CERN site.

Taking as input in the simulations the single-bunch longitudinal emittance out of the SPL instead of the overall emittance, the phase spread at PS injection is ±9° (at 352 MHz) for zero current and ±10° for 40 mA. This value is a measure of the influence of space charge on PS capture. The corresponding residual energy spread is ±0.5 MeV.

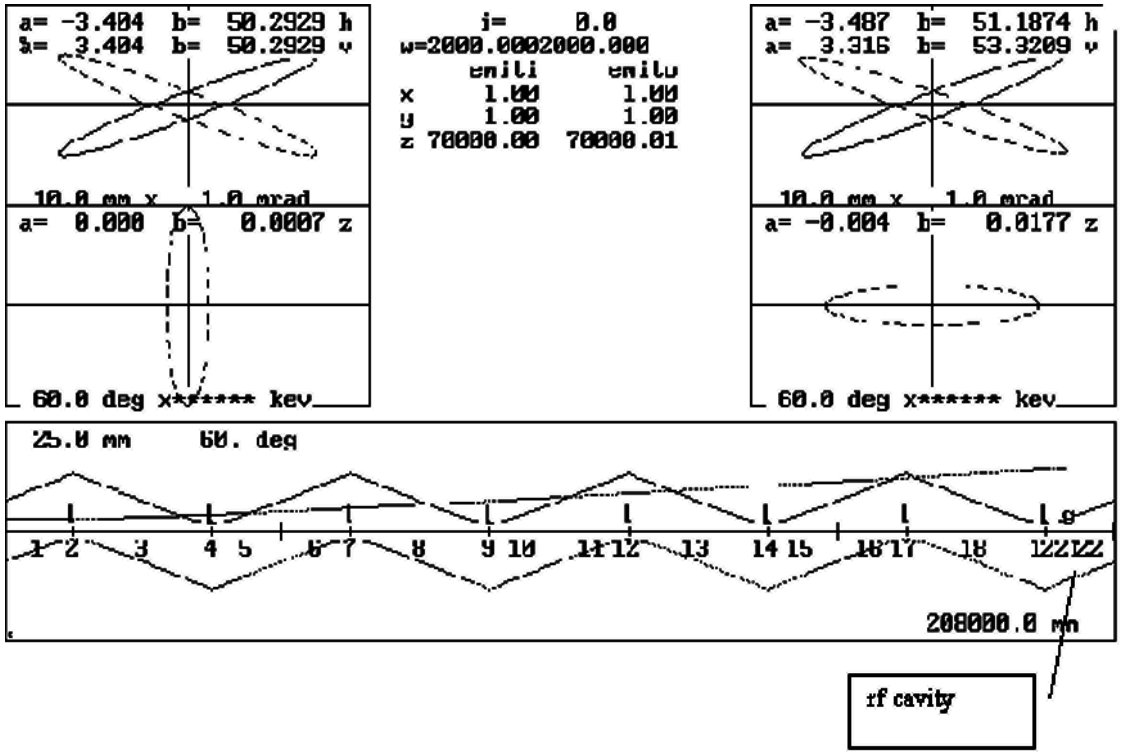

Figure 3.21: TRACE3d run from the exit of the SPL to the entrance of the PS.

3.4 RF and Cryogenics

LEP will be equipped in 1999 with 288 SC cavities (272 of the Nb/Cu type and 16 of the solid niobium type). They are powered by thirty-six 1.3 MW (CW) klystrons (one klystron feeds eight cavities through an array of magic tees) and will deliver a total accelerating voltage of about 3 GV (at $\beta = 1$).

A small fraction of the LEP-2 RF power system will be re-used for the LHC at Point 4, where the accelerating system is located. Eight klystrons and eight circulators (plus spares) are to be modified (or partially rebuilt for a frequency of 400 MHz). The rest, including the high-voltage distribution boxes (one for every two klystrons), the high voltage, high-power converters and a large fraction of the waveguide distribution system with magic tees could be employed for the SPL.

Pulsing the LEP klystrons, as foreseen for the SPL, is certainly possible. It is routinely done during cavity conditioning with RF pulses of about 10 ms duration. However, the very high reflected power from the SC cavities (four times the forward power) at the sharp end of the pulse may cause damage to the circulators. This effect, which led to some design changes in LEP, must be carefully evaluated for a continually pulsed mode of operation. To minimise power consumption, it will be necessary to modify the klystron modulator circuits (which for LEP are relatively slow) to achieve rise and fall times compatible with SPL operation. With a pulsed load, the dc power converters may exhibit some disturbing internal resonances, which would require some (hopefully minor) modifications.

The nominal Q_{ext} value for LEP cavities ($\beta = 1$) is 2×10^6. This corresponds to full power transfer to the beam at an intensity of 10 mA (on the crest of the wave) and an operating field of 6 MV/m (10 MV/cavity), and is therefore adapted to the high-energy sections of the SPL. For the reduced-beta section, where the voltage per cavity gets smaller, an adjustment of the coupling factor (length of the coupler antenna) will probably be necessary. For the same reason the number of cavities fed by the same klystron can be changed from 8 to 16 in the early part of the SCL.

Due to the mechanical tolerances of the cavities (sheet metal construction) and the resulting field flatness imperfections, there is a large scatter in the cavity coupling factors (or Q_{ext}'s) to the waveguides. It has been demonstrated experimentally that correction of the largest Q_{ext} errors can be achieved with simple $\lambda/4$ waveguide transformers located in a long straight section of waveguide upstream of the cavity couplers. Fully adjustable $\lambda/4$ transformers can also be considered (a prototype has been built), but they are quite expensive.

The electrical length of the waveguides, from circulator to the cavities, cannot easily be determined with an accuracy better than a few degrees of RF phase (±5°, including the effect of the couplers themselves, is a typical figure for LEP). It will therefore be necessary to include variable phase shifters in front of each cavity to compensate phasing and coupling tolerances. A design with three movable pistons exists for a limited range (0-60°), but simpler solutions are also possible.

The cryogenic load of the SPL SC cavities is essentially static, the RF and beam-current-dependent losses being negligible at the duty factors considered. The design figures [3.25] are given in Table 3.6.

Experience of pulsed operation of LEP-2 cavities has been acquired over a long period in the SPS (with a pulse length of 250 ms and two to four pulses every 14.4 s cycle). The cryogenic consumption of the "half modules" installed in the SPS corresponds to the above evaluation.

Thermal radiation across superinsulation	4 × 9 W
Conduction in support rods	4 × 2.5 W
Conduction in cooled beam cones	2 × < 1 W
Conduction in cooled main couplers' (MC) extension tubes	4 × < 1 W
Conduction from heated tuners	4 × < 0.1 W
Conduction in pipes	4 × < 2 W
Various smaller loads, including sensor cables and passages across insulation	4 × < 5 W
Typical total module static load	80 W
Equivalent refrigeration load of gas cooling MC, tuners and cones (0.8 g/s)	100 W
Total static refrigeration load per module	180 W

Table 3.6: Static thermal loads of a niobium-film module.

3.5 H^- Stripping

An H^- ion moving through a magnetic field can be stripped to H^0 due to the electric field, *E*, seen in the rest-frame. The neutralisation rate per unit length in the presence of quadrupole magnets can be calculated. The rest-frame lifetime may be estimated from the following expression [3.26]:

$$\tau = \frac{A_1}{E}\exp\left(\frac{A_2}{E}\right) \tag{1}$$

where A_1=2.47 × 10^{-6} Vs/m and A_2=4.49 × 10^9 V/m. Formula (1) has been applied to H^- stripping in the LAMPF PSR [3.27, 3.28]. The electric field is determined by the transverse magnetic field, B, in the rest-frame:

$$E=\beta\gamma cB,$$

where *c* is the speed of light. A quadrupole magnet produces an electric field that is a function of radial position:

$$E = E_0\frac{r}{r_0}$$

where r_o is the beam radius. Hence the H^- beam current loss per unit length of the SPL can be found by integrating over the beam cross-section:

$$\frac{dI(W)}{dz} = I(W)\frac{2E_0\exp(-\frac{A_2}{E_0})}{\beta\gamma cA_1\left(\frac{A_2}{E_0}+4\right)}\frac{L_q}{L_f} \tag{2}$$

where L_q is the doublet length and L_f is the length of the focusing period. For the focusing gradients along the SCL of Figure 3.21 (dotted curve), the relative beam loss

per meter calculated using formula (2) for a constant beam radius of 10 mm inside the quadrupoles is shown in Figure 3.22. For this pessimistic case (the computed beam radius inside the quadrupoles, Figure 3.10, is between 3 mm and 7 mm), the relative loss, $<10^{-9}$/m, is much smaller than the loss limit of the SPL at 5% duty cycle, 10^{-6}/m.

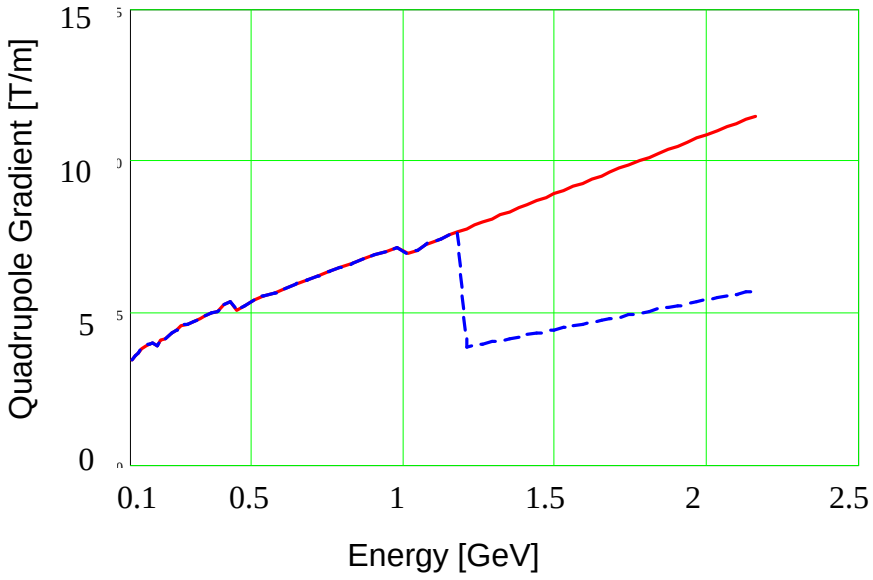

Figure 3.21: Quadrupole gradients along the SCL. The upper curve corresponds to all quadrupoles of 40 cm length, the lower (dotted) curve to 80 cm quadrupoles above 1.2 GeV.

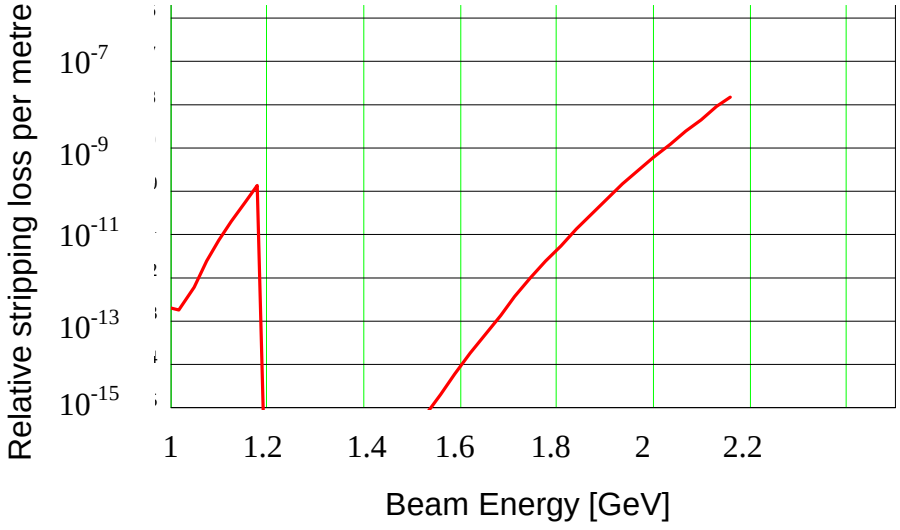

Figure 3.22: Relative stripping loss per meter in the SCL above 1 GeV for 10 mm beam radius (quadrupole gradients corresponding to the dotted curve of Figure 3.21).

The relative current loss when an H^- beam passes through a bending magnet may be found from:

$$\frac{\Delta I}{I} = \left[1 - \exp(-\frac{S}{\gamma\tau\beta c})\right]$$

where S is the beam path length in the magnet. The relative current loss at 2 GeV as a function of magnetic field is shown in Figure 3.23 for 45° and 90° bending angles, taken as test values for the design of the transfer line and of PS injection layout. The bending field should be limited to ~0.2 T, so the beam path in a 90° magnet is ~75 m.

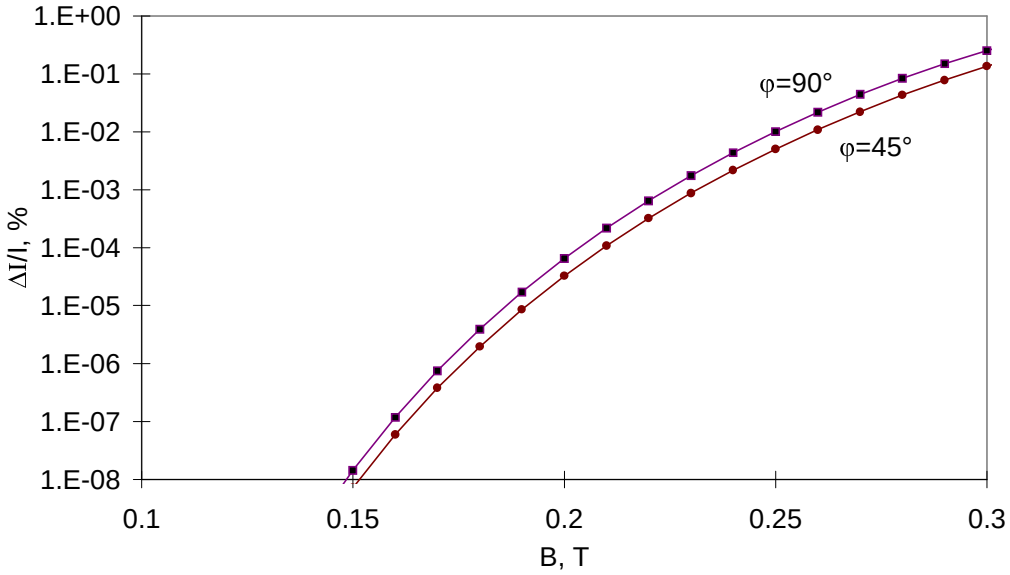

Figure 3.23: Relative current loss in 45° and 90° bends.

4 INJECTION AND CAPTURE IN THE PS

4.1 Basic Considerations

Injection Energy

The PS injection energy should be as high as possible to reduce the transverse tune spread, ΔQ, induced by space charge in the PS [4.1]. Tune spread is the factor limiting beam brightness, N/ε^*. Assuming a round beam,

$$\Delta Q \propto \frac{1}{\beta\gamma^2 B_f} \cdot \frac{N}{\varepsilon^*}$$

where N is the number of circulating protons, ε^* is the normalised rms emittance, B_f is the bunching factor (mean/peak line density), and β and γ are the usual relativistic parameters.

Section 3 shows that, by re-using LEP-2 RF hardware, a kinetic energy of 2 GeV can be achieved at the output of the SPL. Compared with the nominal case for LHC, where the injection energy is 1.4 GeV, the beam brightness can be increased by a factor of 1.6 for the same ΔQ. Given that the intensity required by the LHC is attained in just ~250 μs with the SPL, instead of 1.2 s with the PSB, an increase of the brightness by a factor of 2 is considered feasible [4.2].

Transverse Accumulation

Charge exchange injection is widely accepted as the optimum process for multi-turn injection into a synchrotron. It has the following key advantages:

- high efficiency (low loss) which minimises the current required in the linac and the induced activity in the accelerator,
- minimal transverse emittance of the accumulated beam.

Section 4.2 describes how charge exchange injection may be implemented in the existing PS machine at 2 GeV — an energy where that technique has never previously been employed.

Because of the small SPL beam emittance and of the charge exchange injection process, all the beams needed for the LHC [4.3] are easy to generate by varying the number of turns accumulated:

- with ~20 turns, the characteristics of the commissioning beam can be attained (1.7×10^{10} protons per bunch on h=84, ε^* =0.75 μm);
- with ~65 turns, the nominal beam intensity is obtained, but within half the specified emittance (1.05×10^{11} protons per bunch on h=84, ε^* =1.5 μm);
- with ~110 turns, the intensity of the ultimate beam is achieved, also within half the specified emittance (1.7×10^{11} protons per bunch on h=84, ε^* =1.5 μm).

For the needs of fixed target physics (neutrino experiments, etc.), much higher beam intensities can be obtained using a longer SPL pulse and filling a larger fraction of the aperture. The analysis of charge exchange injection in Section 4.2 treats the case of the present intensity record (3×10^{13} protons per pulse) and shows that this

can be obtained within smaller transverse emittances than today and with much less beam loss.

Longitudinal Accumulation

In order to maximise the longitudinal capture efficiency, the SPL beam is chopped so that particles are only deposited inside PS buckets on h=21. Chopping is such that one bucket is left empty (Figure 2.2), so that the beam can be transformed at high energy into a train of 80 consecutive bunches on h=84 as sketched in Figure 4.8 (Section 4.3.3). This leaves four consecutive unpopulated buckets for the rise-time of the ejection kicker.

4.2 H^- Injection Layout

H^- Injection

The process of stripping H^- into protons using a thin foil at a location where the injected and circulating beams are close together permits continuous injection into the same region of phase space. Intense beams with low emittances can therefore be attained. Calculations from the European Spallation Source (ESS) [4.4] show that an H^- stripping efficiency of 98.5% can be predicted with some confidence. The remaining unstripped H^- and H^0 particles will be eliminated on dedicated dumps.

The first calculations have been made assuming a number of injected protons corresponding to the PS "high intensity" beam, which is equal to about twice the LHC intensity, and a linac emittance of 0.6 μm. For this beam, the full 2 GeV injection process into the PS can be achieved in 250 turns using a linac with a chopper system, providing a total of 3×10^{13} circulating protons within 550 μs and normalised emittance $\varepsilon^*_{x,r}$ = 3 μm. The Twiss parameters of the stored beam at the foil azimuth are $\beta_{x,r}$ = 11.79 m, $\alpha_{x,r}$ = -0.06, $\beta_{y,r}$ = 22.26 m and $\alpha_{y,r}$ = -0.03 (subscripts x and y refer to the horizontal and the vertical planes, i and r denote the incoming turn and the ring respectively). The dispersion at the injection point is $D_{x,r}$ = 2.31 m. The Twiss parameters of the injected beam at the foil are derived from the expressions $\beta_I = \beta_r(\varepsilon_i/\varepsilon_r)^{1/3}$ and $\alpha_i = \alpha_r\beta_i/\beta_m$, yielding $\beta_{x,i}$ = 6.89 m, $\alpha_{x,i}$ = -0.03, $\beta_{y,i}$ = 13.02 m and $\alpha_{y,i}$ = -0.02. Elliptical beam densities in the transverse plane have been considered in subsequent simulations, giving parabolic beam profiles. Beams with truncated Gaussian density in energy have also been considered with a total energy spread of 3 MeV. Limiting phase space ellipses with "radii" of $\sqrt{5}\sigma_r$ and $\sqrt{5}\sigma_i$ contain 100% of the stored and injected beams, which corresponds to 98.4% of the beams within projected dimensions of $\pm 2\sigma_r$ and $\pm 2\sigma_i$.

Transverse injection painting is generally required to minimise the space charge tune shifts. However, Figure 4.1 shows that there is little room for painting the 3 μm PS emittance needed for the LHC with the 0.6 μm SPL emittance. Thus, no painting is carried out, but fixed horizontal and vertical closed orbit bumps of 5.3 and 7.3 mm, respectively, are necessary to separate the closed orbit from the injected ion trajectory. A vertical bump is necessary because the injection foil is of corner shape, i.e. it occupies the upper right corner of the injection plane (third picture in Figure 4.2). The expected tune shifts are very small.

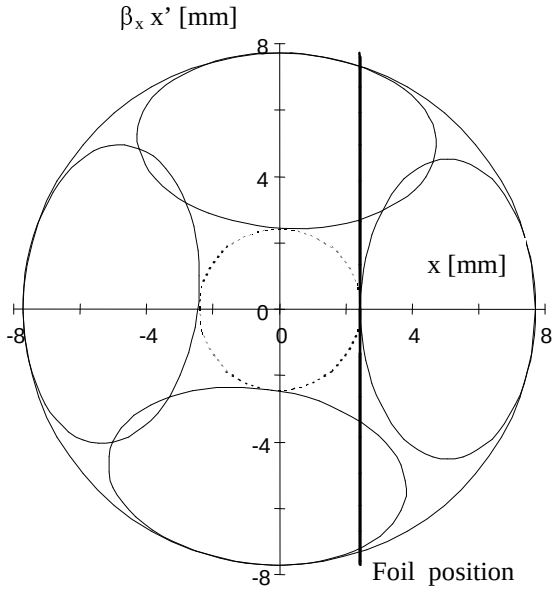

Figure 4.1: Horizontal stored and injected beam ellipses at the injection foil in normalised phase plane $x,\beta_x x'$ (after four injected turns) for PS tunes of $Q_x = 6.24$ and $Q_y = 6.29$. The closed orbit bump amplitude at injection is 5.3 mm. Horizontal physical emittances are $\varepsilon_{x,i} = 1.0$ μm for the injected beam and $\varepsilon_{x,r} = 5.1$ μm for the stored beam (total √5 rms).

Computer modelling of H^- injection has been carried out using the code ACCSIM [4.5]. Carbon corner foils of various thickness have been considered, with and without coupling between the planes. Figure 4.2 shows the ACCSIM scatter plots in transverse and longitudinal phase space and in real space after completion of the injection process using a 450 μg/cm^2 foil (2 μm thickness). For the 250 turns injected, the predicted average number of foil traversals per particle is 30. For this foil thickness the calculated emittance growth is about 7% in the horizontal plane and 15% in the vertical plane. The calculated linear space charge tune shift is about –0.07 in both planes. The G-factor (ratio of the particle density in the beam centre to the average density) of 0.76 found is lower than unity, as expected for a hollow beam. Further simulations should be undertaken to consider the space charge potential of the hollow beam created during the injection. The foil temperature at the end of the H^- injection process has been computed from the energy deposit in foil to be 2320 °C, considering the effects of injected ions and circulating protons scatter in the foil. This temperature rise is well below the 3550 °C melting point of carbon.

Similar simulations of 2 GeV H^- injection have been carried out for stored beams of the same brightness but with half the intensity and transverse emittance. This scheme fills 1.5 μm with 1.5×10^{13} circulating protons in 125 turns using the same 0.6 μm SPL emittance. In this case, the predicted average number of foil traversals per particle is reduced to 20, the emittance increase remains below 8% in both planes and space charge tune shifts do not exceed –0.15.

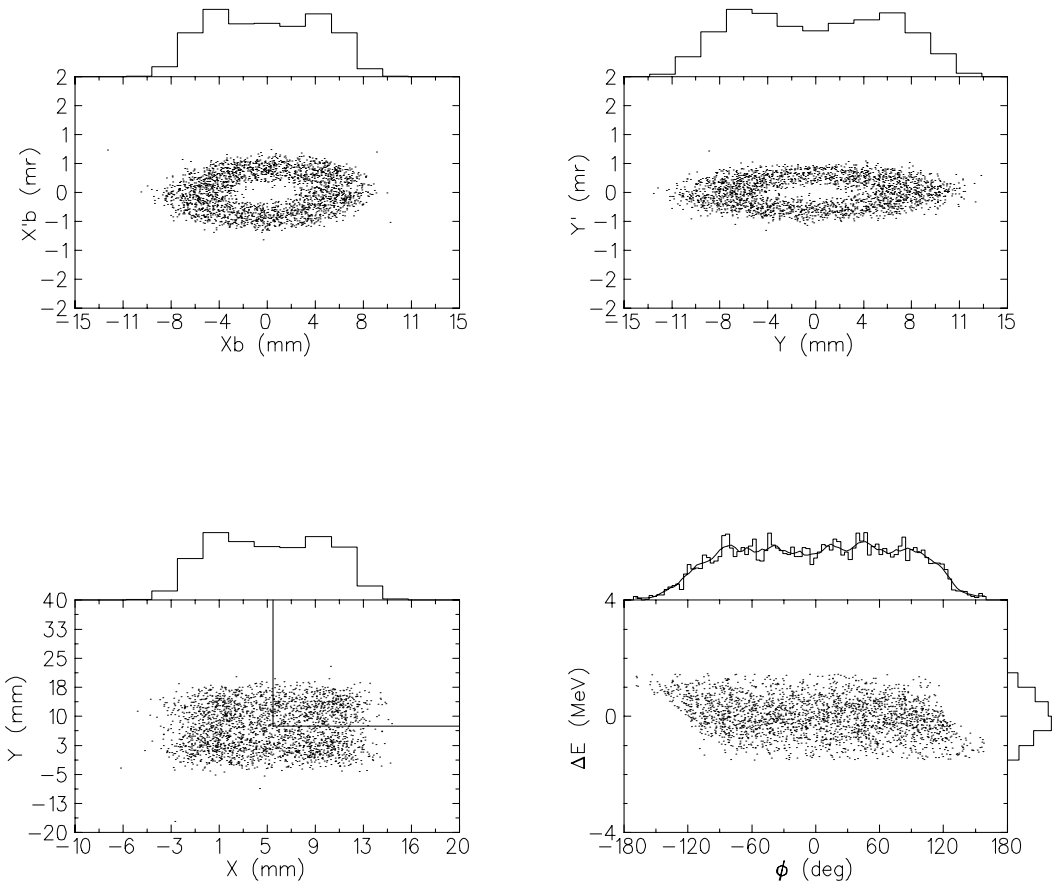

Figure 4.2: ACCSIM plots after the injection of 250 turns into the PS using a 450 $\mu g/cm^2$ carbon foil: transverse phase space (top), real space and longitudinal phase space (bottom). Transverse physical emittances are $\varepsilon_{x,r}(95\%) = 5.0\ \mu m$ and $\varepsilon_{y,r}(95\%) = 5.4\ \mu m$ for the stored beam. For comparison, the emittances would be $\varepsilon_{x,r}(95\%) = 4.7\ \mu m$ and $\varepsilon_{y,r}(95\%) = 4.7\ \mu m$ for a zero thickness foil.

Injection Layout

The H^- injection point is assumed to be in the middle of PS short straight section 60 (1 m long). Combined function magnet units (each 5 m long, including the coil dimension) are interleaved with the drifts. The injection bump is provided by four thin dipoles, one located in short straight section 59 (1 m long), one in straight section 61 (2.4 m long) and two in straight section 60. By tilting these dipole magnets, simultaneous bumps will be made in both planes. The calculated kicks are approximately 1 mrad per dipole. The coupling introduced by the edge effect of tilted dipoles has not been quantified yet. The following injection geometry has been calculated on the basis of the 125-turn injection scheme rather than the 250-turn one, but this does not significantly affect the injection layout. Removal of unstripped H^- ions and H^0 particles can be achieved by using two dumps placed off-centre in long straight section 61 adjacent to the magnet unit 60. Electrons clearing will be completed using an electro-magnet and a collector installed in the vicinity of the foil.

Ion and proton trajectories have been calculated analytically by integrating the equations of motion inside the injection region of the PS. To this end, the measured

field map of a PS magnet has been converted into a polynomial to get a suitable functional form. Figure 4.3 shows the H^- ion and proton trajectories in a Cartesian frame x-z with the origin of the x-axis at the entrance of straight section 59 and the z-axis aligned such that the proton closed orbit enters magnet unit 59 (upstream of the injection straight section) at $x = 0$. The incoming H^- beams enter the injection region at position $x = 427.7$ mm ($z = 0$) and angle $\phi = -88.4$ mrad and hit the foil at $x = -19.6$ mm ($z = 6.799$ m) and $\phi = -31.8$ mrad.

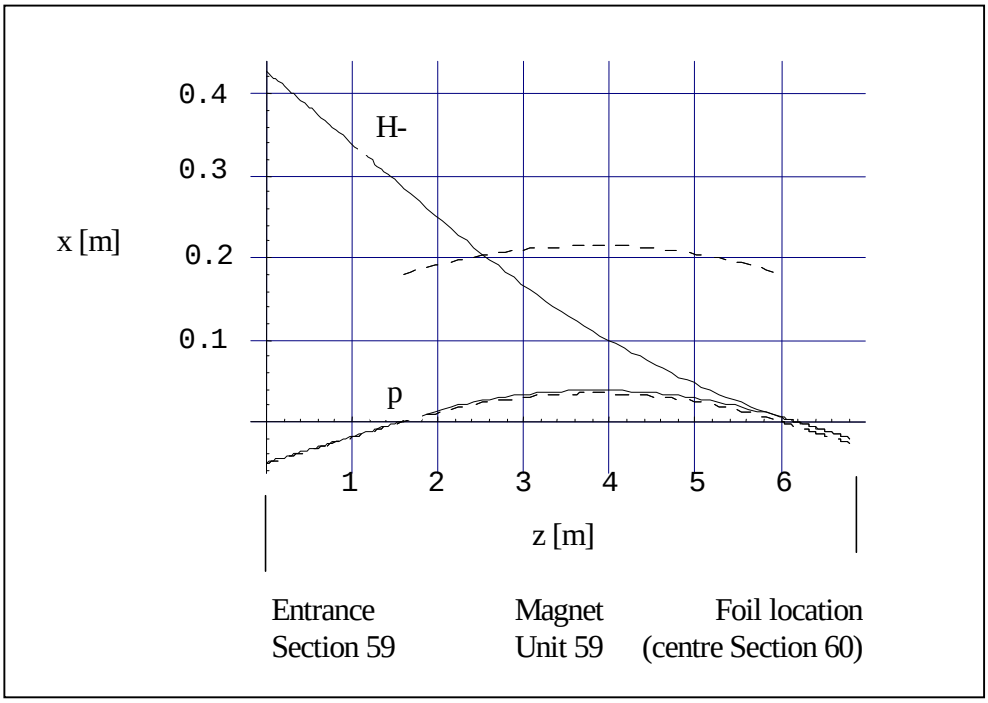

Figure 4.3: H^- trajectory and PS proton closed orbit with bump from straight section 59 entrance up to foil location. The two dotted lines show the PS reference proton closed orbit without bump (bottom) and the outline of the magnet unit 59 yoke (top).

Magnet unit 59 is made of a closed half-unit (which is vertically focusing for negatively charged particles) followed by an open half-unit with the yoke oriented towards the centre of the ring. The field aberrations are strongly non-linear in the closed half-unit since the H^- trajectories pass far from the central orbit, whereas they remain small when the open half-unit is traversed because the H^- trajectories remain close to the central orbit. This results in very large vertical beam sizes at the entrance of this magnet. Given the Twiss parameters required at the foil for optimal H^- injection and using the transfer matrix for small oscillations about the H^- path, the propagated Twiss parameters of the incoming H^- ions evaluated at the azimuthal location corresponding to the entrance of straight section 59 are $\beta_{x,i} = 1.77$ m, $\alpha_{x,I} = 0.05$, $\beta_{y,i} = 67.65$ m and $\alpha_{y,i} = -11.0$. Hence, in order to guarantee the correct optical parameters at the injection foil, two matching quadrupoles will presumably have to be installed at the end of the SPL-to-PS transport channel.

4.3 Longitudinal Capture

An important issue for the injection of a high intensity beam into the PS is the control of space-charge effects. This holds especially for the 160 ps long SPL bunches, where the peak charge density is particularly important. In order to counteract the space charge defocusing, the applied RF voltage has to be high as compared to the space charge voltage, which reaches high local values for very short bunches.

The underlying equations to numerically treat the synchrotron motion are

$$\frac{d}{dt}\frac{\Delta \mathrm{E}}{\omega_0} = \frac{q}{2\pi}\left[V(\varphi) - V(\varphi_s) + V_{SC}(\varphi)\right]$$

$$\frac{d}{dt}\Delta\varphi = \frac{h\omega_0\eta}{\beta^2 E_s}\Delta E$$

where $\Delta E = E - E_s$, $\Delta\varphi = \varphi - \varphi_s$, $\eta = 1/\gamma_t^2 - 1/\gamma^2$ with γ_t gamma at transition. E and φ are the energy and the phase of the particle, $V(\varphi)$ is the applied RF-voltage and h the harmonic number. The suffix s refers to the synchronous particle and, since the equations govern only first-order variations from the synchronous values, the revolution frequency ω_0 is evaluated for the synchronous particle in the calculations. The space-charge voltage V_{SC} generated within the beam is given by the derivative of the line density $\lambda(\varphi)$ of the particle distribution

$$V_{SC}(\varphi) = -q\frac{d\lambda(\varphi)}{d\varphi}\cdot\frac{Rg_0}{2\varepsilon_0\gamma^2},$$

where R is the radius of the machine. For a beam with circular cross section of mean radius a in a circular pipe of radius b, the geometry factor g_0 factor is defined as $g_0 = 1 + 2\ln(b/a)$. The inductance L of the vacuum chamber wall may be neglected in the present problem.

A modified version of the multi-particle tracking code TRACK1D [4.6] has been used for the simulations. The main modifications consisted in 1) allowing the injection of many bunches at variable distance, corresponding to different linac filling factors, in the same synchrotron bucket [4.7], and 2) allowing the phase of the injected bunches to shift gradually from one turn to the other. The latter represents the fact that linac and PS RF frequencies will not be synchronised. In this way, the linac bunches are not injected one over the other, and the overall space charge potential is reduced.

In the simulations, the total number of protons in the ring is 1.5×10^{13} and the injection of the 10 mA mean current SPL beam covers 110 turns. This beam is represented by up to 150000 macro-particles. The initial longitudinal particle distribution injected in every bucket consists of 11 bunches of parabolic phase and momentum distribution spaced by 19.4° at the 9.5 MHz PS RF frequency and with a total energy spread of ±0.7 MeV. The centre phase of each bunch shifts by 18° (1/20 of the period at 352 MHz) at every turn, to simulate the effect of asynchronous RF frequencies. The parameters of the PS machine are radius of 100 m, bending field at injection of 0.1327 T and bending radius of 70 m. The RF harmonic number is 21 and the fixed RF voltage is 50 kV.

Two different cases have been analysed. In the first one, the linac bunches are injected at the correct energy, 2 GeV. In the second case, they are injected with an

energy offset of 1.5 MeV, corresponding to 3 times the rms energy error introduced by mechanical vibrations in the superconducting cavities with ±20 Hz maximum detuning (Section 3.2.4 and Figure 3.20). The rotation of the effective longitudinal emittance by the energy-correcting cavity (Section 3.3) is taken into account.

From the simulations one can see that the line density of the beam builds up during beam accumulation and reaches its peak value right at the end of the injection process, when many bunches are still upright in longitudinal phase space. After more turns, the bunches rotate inside the bucket and smear out filling the entire bucket area. Consequently, the first few turns right after injection are the most critical ones. Peak line density and space charge voltage rapidly decrease as times goes on.

The evolution of the phase space distribution during injection is represented in Figures 4.4 and 4.5, the latter for the case with energy offset. The RF bucket for zero space charge is drawn to guide the eye, and a darker shadow corresponds to higher particle density. Figures 4.6 and 4.7 show the corresponding phase space snapshots, including for comparison the case without space charge, together with line density and space charge voltage after ~11 synchrotron periods (4900 turns). The computed capture loss is zero for injection at the correct energy, and in the case with maximum energy offset less than 1% of the particles lie outside of the bucket. The overall computed capture loss in case of linac cavity vibrations of ±20 Hz is therefore $<10^{-3}$.

More work is now required to finally tune the RF voltage during capture and optimise the process in the longitudinal phase plane. Moreover, the use of a VHF RF has to be studied, to help speed up the dilution of the beam in the buckets and smoothen the charge line density.

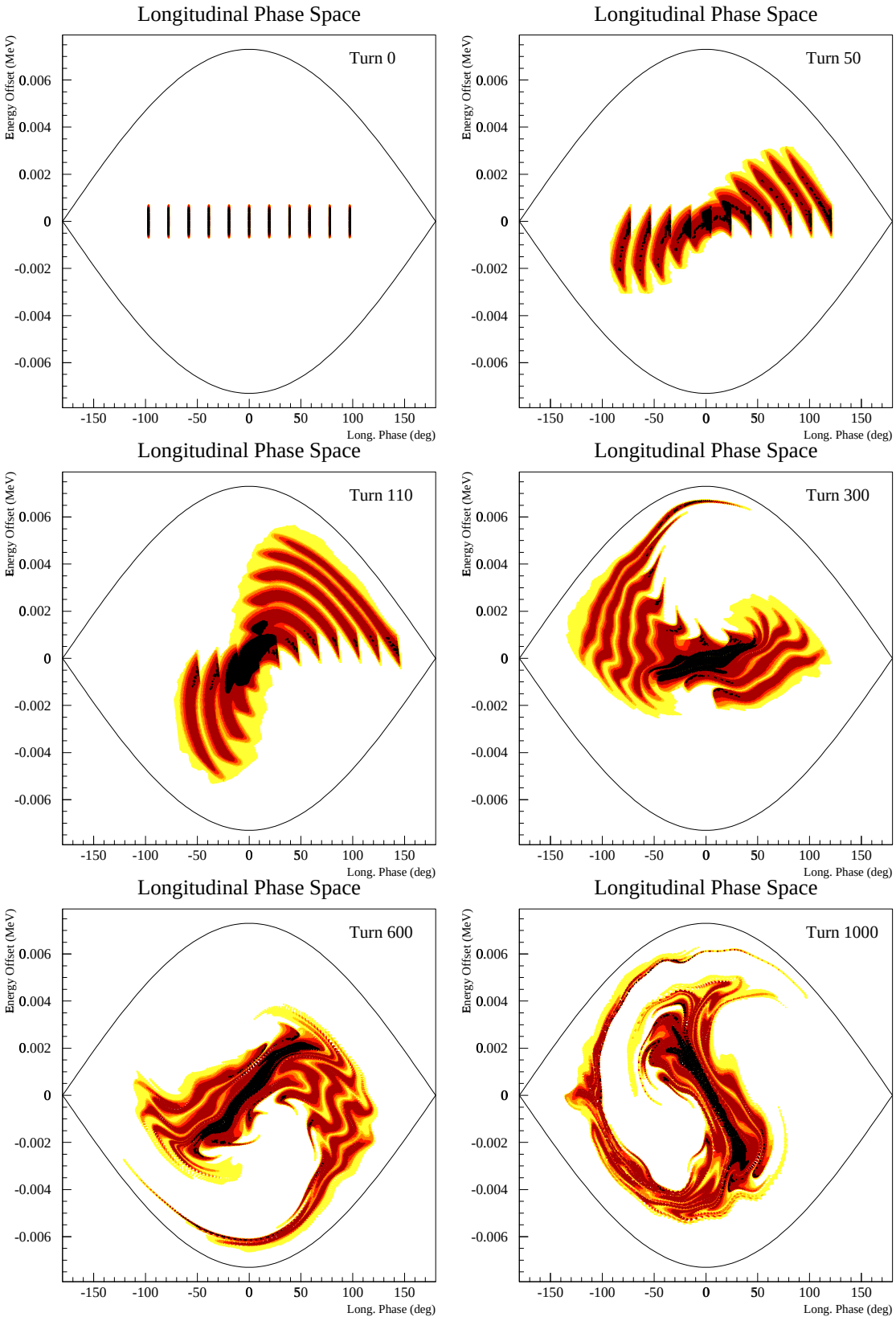

Figure 4.4: Evolution of the particle distribution in longitudinal phase space during the first 1000 turns. The injection ends at turn 110.

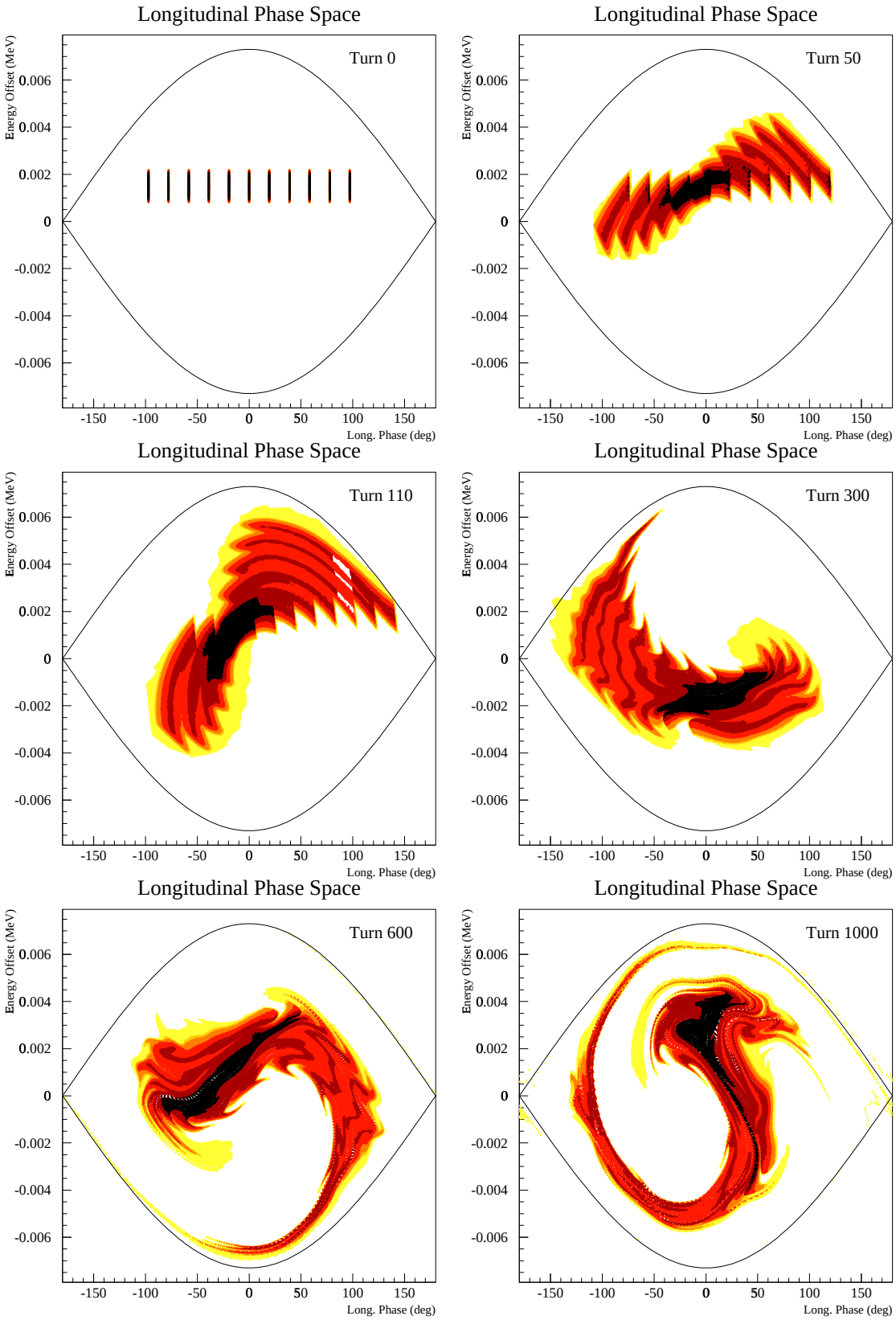

Figure 4.5: Evolution of the particle distribution in longitudinal phase space during the first 1000 turns, for an offset in energy at injection of +1.5 MeV. The injection ends at turn 110.

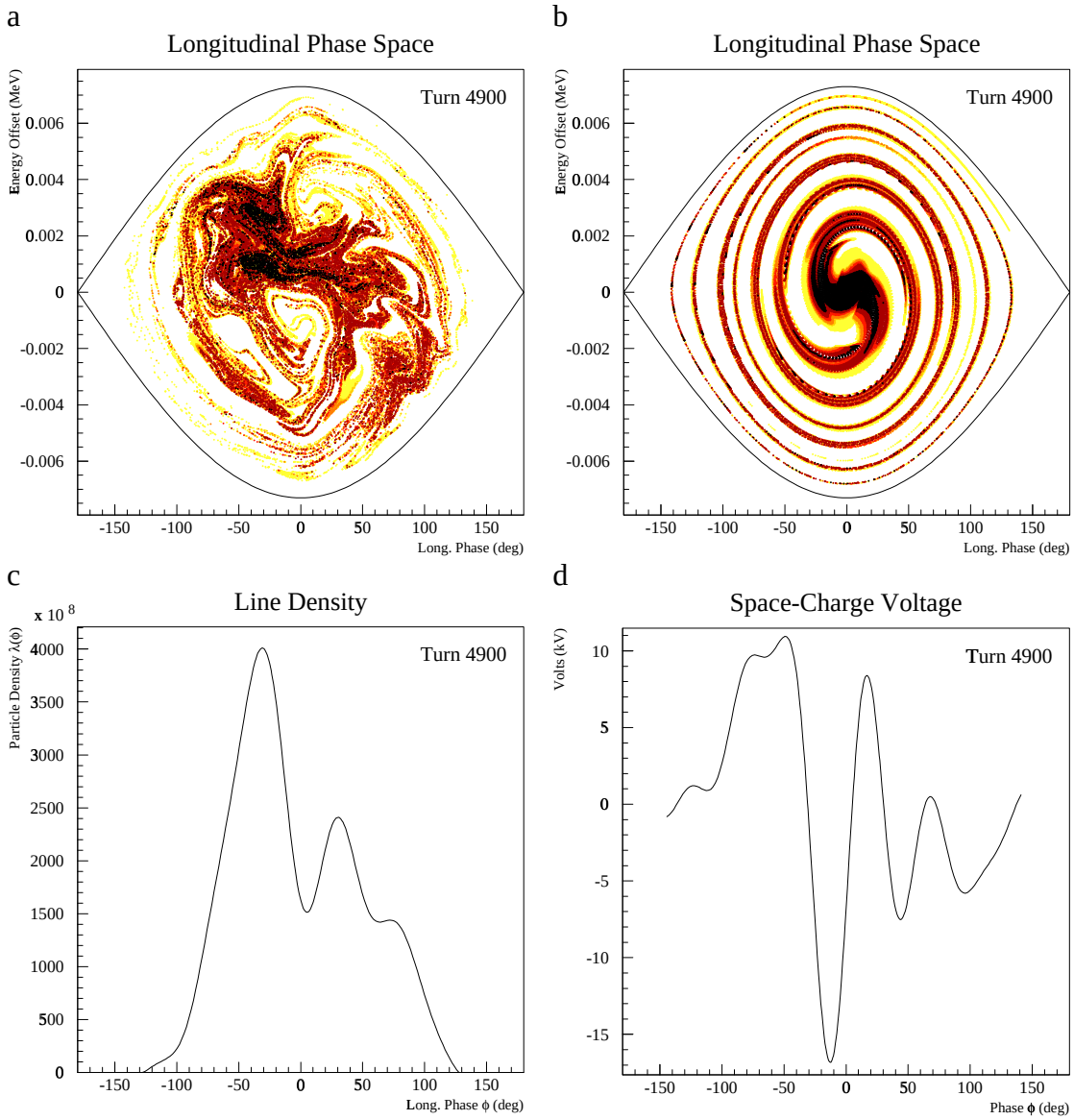

Figure 4.6: Population of the longitudinal phase space after 4900 turns, with (a) and without (b) inclusion of space charge effects. The line density and space charge voltage for situation (a) are drawn in (c) and (d).

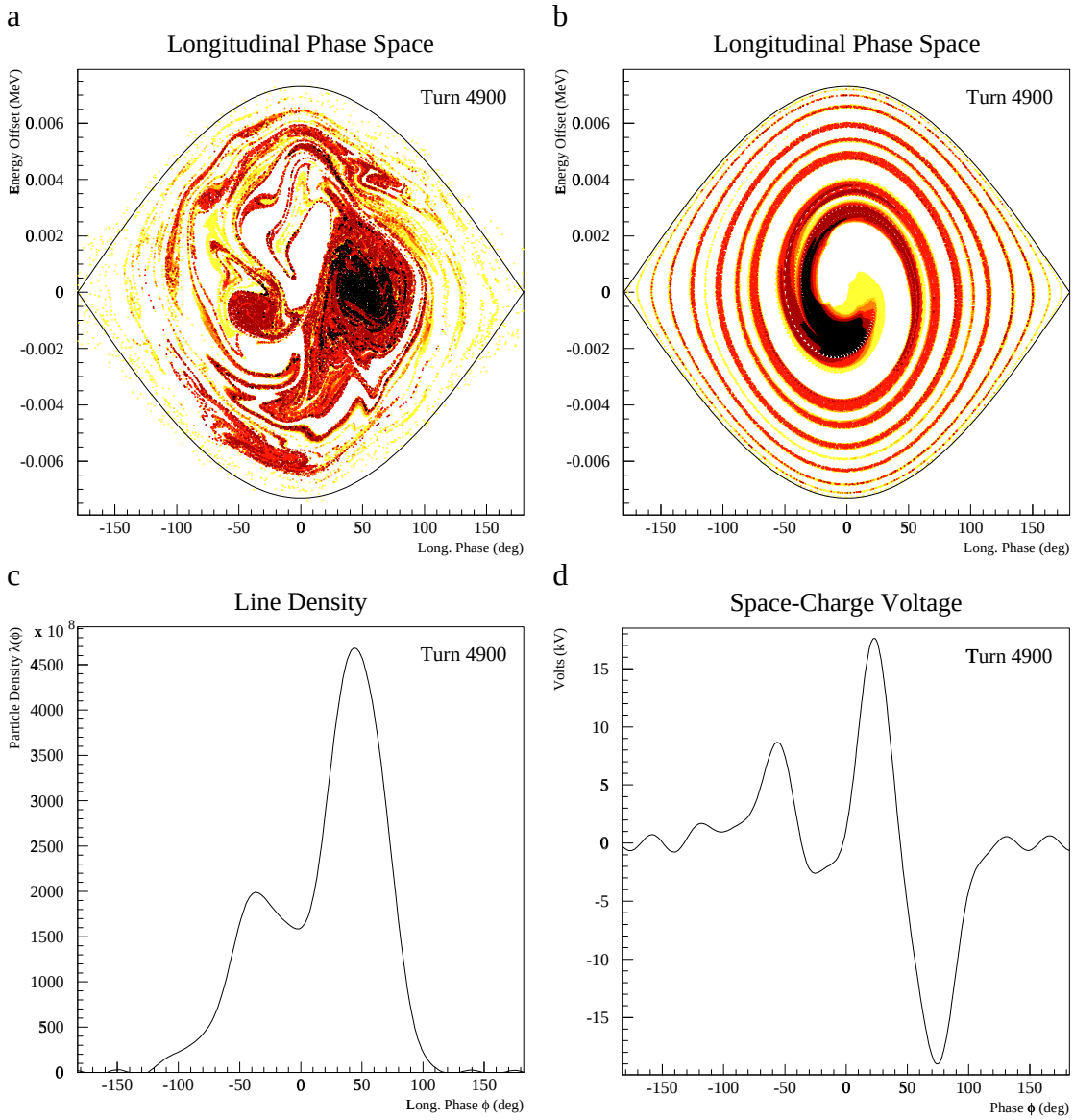

Figure 4.7: Population of the longitudinal phase space after 4900 turns, with (a) and without (b) inclusion of space charge effects, for an offset in energy at injection of +1.5 MeV. The line density and space charge voltage for situation (a) are drawn in (c) and (d).

4.4 Acceleration and Beam Gymnastics

Once bunches are formed at 2 GeV, acceleration takes place on harmonic *h*=21. The PS having already demonstrated in the past its capability to accelerate beams with similar longitudinal characteristics on harmonic *h*=20, no difficulty is expected in the longitudinal phase plane for any of the beams required by the planned high energy physics programme.

For the generation of the beam required by LHC, double bunch splitting will permit the avoidance of the problems associated with passing through a debunched beam state and keep a gap for kicker rise-time in the bunch train. Figure 4.8 shows the proposed evolution of the longitudinal particle density at 26 GeV in the PS. Twenty bunches held in *h*=21 buckets are adiabatically "split" twice. This gives first 40 bunches in *h*=42 buckets, then 80 bunches in *h*=84 buckets.

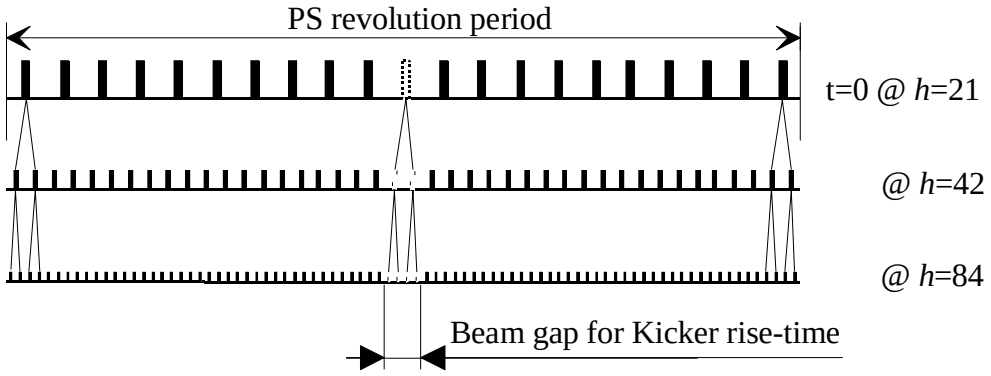

Figure 4.8: Evolution of beam longitudinal density at 26 GeV.

Bunch splitting has been amply demonstrated [4.1] and has the remarkable capability to preserve the total longitudinal beam emittance.

5 OTHER APPLICATIONS

5.1 Potential of the Facility

The previous sections have dealt with the performance of the PS for the presently planned CERN physics programme, and especially for LHC. But the 2 GeV Linac can potentially provide 1 ms beam pulses every 20 ms that can be used either directly or through the PS. Both uses can be interleaved in time.

Direct uses of the SPL beam

The possibility to make use of the Linac beam for a radioactive ion source like ISOLDE is considered in Section 5.3, where the possible extension of the existing facility is envisaged, as well as the future needs of the next generation of sources.

This beam is also of interest for driving a neutron spallation source as described in Section 5.2. Its potential performance is compared to the existing proposals.

Beam uses through the PS

The first direct consequence of the 50 Hz SPL repetition rate is that the dead time in each PS cycle can be reduced to a minimum because the repetition period does not necessarily need to be a multiple of 1.2 s, as imposed today by the PSB. The flexibility introduced in the programming of the PS cycles will help increase the mean current delivered by the PS, even if the intensity per cycle is kept constant.

Moreover, the PS proton intensity per cycle can be increased well above the present limit of 3×10^{13}. Making use of the 1 ms beam pulse length capability of the SPL and using the nominal parameters for longitudinal capture (chopping as in Figure 2.2), beam can be accumulated over ~450 turns. This corresponds to 6.25×10^{13} circulating protons in 20 bunches on h=21, which might be of interest for new physics experiment needing high flux from the PS (neutrino experiments, etc.), especially if use is made of the flexibility introduced by the cycling rate. Such flexibility would also make the PS an invaluable test bench for machine studies with a view to future high intensity machines (neutron spallation sources, proton driver for a muon collider, etc.).

Another interesting benefit comes from the wide-band chopper that allows to populate the PS bunches in an arbitrary manner and, for example, to easily change their number and the distance between them. Using the smallest possible harmonic number compatible with the present ferrite cavities at 2 GeV (h=6), and for the same mean beam current in the Linac, a single PS bucket can collect up to 36 consecutive SPL bunches. With a 1 ms beam pulse, that bunch will accumulate 1.59×10^{13} particles. Provided the PS is equipped with the adequate injection and ejection systems to operate at 50 Hz, these high single-bunch intensities are already very near the expectations of the neutron spallation community. Keeping the present maximum tolerated level of uncontrolled beam losses at 10^{12} protons/s, the percentage of beam lost is at the levels indicated in column 4 of Table 5.1. If this specification is met, the characteristics listed in Table 5.1 can then be expected.

No. protons per pulse	Kinetic energy	Pulse length (at PS extraction)	Tolerable losses	Cycling rate	Mean beam current	Mean beam power
6.25×10^{13}	2 GeV	< 2.2 μs	2×10^{-4}	50 Hz	500 μA	1 MW
1.59×10^{13}	2 GeV	< 360 ns	1.2×10^{-3}	50 Hz	127 μA	250 kW

Table 5.1: High intensity after accumulation in the PS.

Mixed Operating Mode

Table 5.2 shows a typical scenario of operation for the SPL/PS Complex assuming that the SPL pulses at 50 Hz and, somewhat arbitrarily, that high energy physics fills only 60% of the PS schedule.

Beam user	Machine time	Beam characteristics	Beam power
High energy physics (including LHC)	PS: 60% SPL: 0.6%	High energy	
Neutron source	PS: 40% SPL: 40%	50 μA (360 ns) @ 2 GeV or 200 μA (2.2 μs) @ 2 GeV	100 kW or 400 kW
ISOLDE (second generation)	PS: 0% SPL: 59.4%	< 300 μA @ 2 GeV	< 600 kW

Table 5.2: Typical operating modes of the SPL/PS Complex.

5.2 Proton Factory for a Neutron Facility

The linac described in this report could be operated at a duty cycle of up to 5% without major modifications on the cavities and RF generators, so that pulses of, for example, 1 ms at a repetition rate of 50 Hz seem possible.

One possibility of using such a high duty cycle is neutron production with a spallation target. Neutrons play an increasing role in materials research, which is a field covering a wide range of applications ranging from physics, engineering and chemistry to biology and biotechnology. For some 4000 scientists in Europe, neutron beams have become an indispensable tool for their research programmes [5.1]. However, in contrast to the increasing demand from users, there is a predicted decline in the number of neutron sources. The planned NSS in the US and the projected ESS and Austron facilities in Europe try to offer new possibilities. Unfortunately only the NSS is approved at the moment. The ESS is aiming at a beam power of 5 MW, while the NSS is originally foreseen for 1 MW with a possible future upgrade to 2 or 4 MW, and Austron is planned with 400-500 kW at 50 Hz. For comparison we note that the SINQ at PSI operates with a beam power of about 500 kW and ISIS with 200 kW.

The SPL, with a mean beam current of 10 mA at 2 GeV and with a duty cycle of 5%, has a beam power of 1 MW. Consequently, it lies very much in the range of

interest of the neutron-user community. It must be pointed out in this context that a pulsed source has definite advantages compared to a reactor [5.2]. Although there are users for millisecond pulses, quite a strong community needs shorter pulses like 50-100 μs or even down to 10-20 μs [5.2]. It must be remembered that the neutron pulse is lengthened due to the action of the moderator (to produce thermal or even much colder neutrons). Hence, to achieve a 10 μs pulse for example, the proton pulse must not be longer than a few microseconds. However, since the maximum repetition rate is limited (compare the ESS scenario!) to about 50 Hz by the experiments, any shortening of the pulses will reduce the available intensity. An increase in beam current by, say, a factor of ten would yield a higher mean power in spite of such shorter pulses, however a better option would be to use the Booster as an accumulator ring. As this machine would no longer be needed by the PS (at least, for filling the LHC with protons), it could be used exclusively for a neutron production facility. Storing 6.25×10^{13} protons and running at 50 Hz seem feasible at an energy of 1.334 GeV [5.3], corresponding to a beam power of 667 kW. Another, cheaper, option is to use the PS when it is not occupied as an injector for the LHC. As this is the case for most of the time (LHC fillings are relatively brief and infrequent) and as the injection line already exists, no further investment is necessary apart from the usual complications of high power machines e.g. the corresponding need for fast beam dumps and loss control. In addition, it would make use of the full 2 GeV energy. One disadvantage of the use of the PS is of course that it will not only be needed for filling the LHC but also for other beams, which may require perhaps up to a total of 60% of the available time. Building a special compressor ring could lift these limits. Some of the different options are summarised in Table 5.3.

Scenario	Energy [GeV]	Current [mA]	Pulse length [μs]	Repetition rate [Hz]	Total power [kW]
Linac only	2	10	3	50	3
Linac only	2	10	20	50	20
Linac only	2	10	100	50	100
Linac only	2	10	1000	50	1000
With PS	2	≈ 5000	≈ 2	50	≈ 1000

Table 5.3: Neutron production scenarios.

In the case of operation without the Booster or PS, an increase of the SPL proton current to more than 50 mA would not be out of the question. Only the low energy part of the SPL would need to be replaced. This could yield an increase in total power by more than a factor of five.

In the case of operation with the PS, current increases (and hence power increases) of some considerable factor do not seem to be excluded. This could be achieved by upgrading the ion source (a factor 2 in current is a straightforward possibility) and by funnelling. With funnelling, a current increase of a factor of two is achieved by filling all SPL buckets, bringing the total power up to 2 MW. The increase in the source current would result in 4 MW power.

In any case, the critical limit will be the particle losses that can be tolerated. More detailed work is necessary to assess this.

5.3 Driver for the Production of Intense Radioactive Ion Beams

Much effort is presently being invested to plan and develop new facilities for the production of radioactive nuclear beams (RNB) and to further improve existing ones. The scientific potential of intense radioactive ion beams has been recognised world-wide and is the subject of several studies. In the 1996 DOE/NSF NSAC Long Range Plan for Nuclear Physics [5.4], highest priority after RHIC was given to an advanced ISOL facility and a recent report [5.5] summarises the opportunities of such a facility. The Nuclear Physics European Collaboration Committee (NUPECC) has to date reviewed and investigated in several exercises the scientific highlights and perspectives of using radioactive ion beams [5.6-5.8]. Existing and planned RNB facilities have been compared and evaluated [5.9] and a new NUPECC study group has started to investigate the conditions and options for the next generation of radioactive beam facilities in Europe. In addition, the Megascience Forum of the Organisation for Economic Co-operation and Development has recently established a working group on radioactive ion beams to discuss the opportunities for international co-operation in the use of current facilities and the planning of new ones. The common goal world-wide is the production of radioactive ion beams with intensities which are orders of magnitude higher than those presently available. A basic requirement for this is the availability of high intensity driver accelerators.

The ISOL technique has turned out to be a particularly powerful one for the production of intense radioactive ion beams. Several first-generation ISOL facilities are in operation or under construction which use different primary beams for the production of the radioactive species. Some examples are: thermal neutrons at the FRM/Munich, fast neutrons at ANL/Argonne, heavy ions at SPIRAL at GANIL/Caen, IGISOL/Jyväskylä and LISOL/Louvain-la-Neuve, high energy protons at ISAC at TRIUMF/Vancouver, SIRIUS/Rutherford and at ISOLDE/CERN.

For more than 30 years ISOLDE has been the pioneering and world-leading ISOL-type radioactive beam facility connected to a proton accelerator [5.10]. The large number of good-intensity, low-energy radioactive ion beams available today affords a rich physics programme, ranging from nuclear structure studies and atomic physics to condensed matter physics and biomedicine. With the advent of the REX-ISOLDE post-accelerator, a new domain of research will be opened employing nuclear reactions involving energetic radioactive ions.

ISOLDE is presently the user of most of the protons accelerated by the PS Booster. With the SPL, the continued operation of ISOLDE will be possible without any disadvantages. For the same average beam intensity as that delivered today, the yields will be similar to those achieved at the old Synchrocyclotron and at the PS Booster. Furthermore, both on-line mass separators could be operated in parallel without a reduction of the proton beam intensity. This should, in principle, double the productivity of ISOLDE. However, the possibility to increase the average proton intensity on the ISOLDE targets can only be partly exploited with the existing systems and technology.

The ISOLDE ion source targets were designed for, and are presently used at, an average beam intensity of a few μA. For many targets, a higher power dissipation due to larger proton beam intensities would lead to their destruction or to a performance reduction and would not result in higher radioactive beam intensities. Nevertheless, there exist refractory element targets (e.g., the RIST test target developed in

collaboration with the Rutherford Laboratory) which can be used at higher proton beam intensities and which are expected to give a corresponding increase in radioactive beam intensity. With the SPL and the present ISOLDE, the possibility to increase gradually the proton beam intensity beyond the present limit would permit a systematic investigation of target properties as a function of beam intensity. Such tests would be extremely helpful for the design of future high intensity targets. Furthermore, thinner targets with better release properties could be used to provide higher yields for very short-lived isotopes. Consequently, a gain in beam intensity can be expected for a number of radioactive species already in this first stage, with direct benefits for the ISOLDE physics programme.

However, for proton beam intensities exceeding several tens of microamperes, a complete redesign of the ISOLDE target and front-end area and equipment has to be envisaged. Strongly re-enforced radiation shielding will be required and procedures for the safe handling of the much larger amounts of radioactivity produced will have to be established. This and the development of ion sources for high intensities will require a major and expensive R&D effort. However, there are a number of good arguments for an upgrade of ISOLDE compared to building a new facility somewhere else in Europe: a lot of expertise on the ISOL technique exists at CERN; the experimental facilities at ISOLDE are world-class and remain operational; the primary proton beam could be shared in an ideal way with other activities at CERN; and CERN provides the environment for research on an international level.

In conclusion, the conversion of ISOLDE from a first-generation into a high-intensity, second-generation facility is certainly one of the most promising options to be studied. An intense primary beam accelerator like the proposed SPL would be the prerequisite.

6 CONCLUSIONS

The basic technical issues regarding the feasibility and performance of the PS complex equipped with a 2 GeV Superconducting H^- Linac built from LEP-2 hardware have been addressed. Solutions, although in some areas not yet optimised, are proposed. The RF cavities to cover the energy range between 1 and 2 GeV, other major cryogenic components and the RF infrastructure for the complete 2 GeV linac can be recuperated from LEP, leading to a cost-effective machine. The main elements to be constructed are: a 100 MeV room temperature linac, new superconducting cavities and cryostats from 100 MeV to 1 GeV, the focusing and diagnostics equipment, and a 13 kW cryoplant. The facility needs 900 m long tunnel and technical gallery to be built on the CERN Meyrin site, while the transfer lines could use existing tunnels and part of the ancillary equipment could probably be housed in existing surface halls.

A large amount of work is still needed before a detailed design and a cost estimate referring to a precise layout on the site can be prepared. At the present status of the work, this study comes to the following conclusions, for the three possible uses of this new injector linac:

1. For the needs of the planned physics programme at CERN (LHC) the feasibility of that facility is established, and an increase in the beam brightness from the PS complex by a factor 2 can be reasonably expected.

2. Making use of the capability of the linac to deliver more beam than needed by the main CERN physics programme, the PS can either accelerate intensities much higher than the present 3×10^{13} protons per cycle, which can be of interest for example for a new generation of neutrino experiments, or be used as an accumulator for a medium size neutron source at a beam power between 100 and 400 kW. This option requires a stringent control of beam loss and is immediately feasible if the losses in the PS can be kept below 10^{-3} (for 250 kW beam power). For higher loss levels, additional investment would be needed to adapt the PS ring to the higher radiation environment. The linac alone can feed an experimental area for a second generation ISOLDE experiments, where development is needed in order to build and maintain a highly radioactive target area.

3. By fully using the capability of the linac to deliver 1 MW or more of beam, a modern spallation neutron source can be built on the CERN site. The PS Booster could be transformed into a four-ring accumulator/compressor at 1.4 GeV, reaching a beam power of 0.6-1 MW. Alternatively, a new pulse compressor ring can be built for 2 GeV energy and >1 MW beam power. In both cases, modern collimation schemes are required to stand the high loss level. This option, which requires no changes to the linac, is considered in this study but has not yet been the subject of a detailed technical analysis. However, it is considered as an important factor in favour of a Superconducting Proton Linac.

7 ACKNOWLEDGMENTS

The authors wish to thank G. Bollen for writing the Section on radioactive beams, C. Prior (DRAL) and K. Bongardt (KFA-ESS) for their contribution to the study, S. Hancock for linguistically checking the manuscript, P. Bryant for critically revising the paper and finally D.J. Warner for making a thorough critical appraisal of the paper which has led to some modifications in this final version.

8 REFERENCES

Section 1

[1.1] R. Garoby, M. Vretenar, "Proposal for a 2 GeV Linac Injector for the CERN PS", PS/RF/Note 96-27.

[1.2] R. Corsini, A. Hoffmann, "Considerations on an FEL based on LEP superconducting cavities", CERN/PS 96-04.

[1.3] C. Rubbia, J.A. Rubio, "A tentative programme towards a full scale energy amplifier", CERN/LHC 96-11.

[1.4] D. Boussard, E. Chiaveri, G. Geschonke, J. Tuckmantel, "Preliminary Parameters of a Proton Linac using the LEP 2 RF System when Decommissioned", SL-RF Technical Note 96-4.

[1.5] C. Pagani, G. Bellomo, P. Pierini, "A high Current Linac with 352 MHz SC Cavities", Proceedings of the 1996 Linac Conference, Geneva, p. 107.

[1.6] R. Cappi, R. Garoby, S. Hancock, M. Martini, J.P. Riunaud, K. Schindl, H. Schonauer, "Beams in the PS Complex during the LHC Era", CERN/PS 93-08 (DI), 1993.

[1.7] The LEP 2 Team, "LEP Design Report", Vol. III - LEP 2, CERN-AC/96-01 (LEP2).

Section 2

[2.1] J.M. Brennan, L. Ahrens, J. Alessi, J. Brodowski, J. Kats, "A Fast Chopper for Programmed Population of the Longitudinal Phase Space of the AGS Booster", Proc. of the 1988 EPAC, p1003.

[2.2] A. Mosnier, J.M. Tessier, "Field Stabilisation Study for TESLA", DAPNIA/SEA Note 94-07.

[2.3] K. Bongardt, private communication.

[2.4] The European Spallation Source Study, Volume III, The ESS Technical Study, ESS-96-53-M (1996).

[2.5] S. Nath, J. Billen, J. Stovall, H. Takeda, L. Young, "Physics Design of APT Linac with Normal Conducting RF Cavities", Proc. of the 1996 Linac Conference, Geneva, p. 689.

[2.6] R. Garoby, M. Vretenar, "Proposal for a 2 GeV Linac Injector for the CERN PS", PS/RF/Note 96-27.

Section 3

[3.1] Proceedings of the 19th International Linear Accelerator Conference, Chicago, 1998, http://www.aps.anl.gov/conferences/LINAC98/Proceedings-new.html.

[3.2] Proceedings of the 18th International Linear Accelerator Conference, Geneva, CERN 96-07, 1996.

[3.3] Proceedings of the 5th. European Particle Accelerator Conference, Stiges, 1996, IoP Publishing, 1996.

[3.4] Proceedings of the 1995 Particle Accelerator Conference, Dallas, 1995.

[3.5] Proceedings of the 7th International Conference on Ion Sources, Taormina, 1997, Rev. Sci. Instr, 69, 2, part 2, 1998.

[3.6] J. Peters, "The Status of Desy H^- Sources", Proc. of the 18th International Linear Accelerator Conference, Geneva, CERN 96-07, 1996, p199.

[3.7] J. Peters, "Review of Negative Hydrogen Ion Sources High Brightness/High Current", Proc. of the 19th International Linear Accelerator Conference, Chicago, 1998, FR1003.

[3.8] K. Volk, A. Maaser, H. Klein, "The Frankfurt H- Source for European Spallation Source", Proc. of the 19th International Linear Accelerator Conference, Chicago, 1998, THP4057.

[3.9] J.M. Brennan, L. Ahrens, J. Alessi, J. Brodowski, J. Kats, "A Fast Chopper for Programmed Population of the Longitudinal Phase Space of the AGS Booster", Proc. of the 1988 European Part. Acc. Conf., p1003.

[3.10] The European Spallation Source Study, Volume III, The ESS Technical Study, ESS-96-53-M (1996), p. 2-17.

[3.11] T. Kato, "Proposal of a Separated-Type Proton Drift Tube Linac for a Medium-Energy Structure", KEK-Report-92-10 (1992).

[3.12] J. Billen, F. Krawczyk, R. Wood, L. Young, "A New RF Structure for Intermediate Velocity Particles", Proc. of the 1994 Linac Conference, Tsukuba (1994).
[3.13] G. D'Auria, C. Rossi, "A 100 MeV Multitank Drift Tube Linac for Proton Acceleration", Proc. of 1997 Particle Acc. Conf., Vancouver (1997).
[3.14] L. Picardi, C. Ronsisvalle, A. Vignati, "Progetto di Acceleratore Compatto per Terapia Oncologica con Protoni (TOP)", RT/INN/95/22, ENEA (1995).
[3.15] M. Vretenar, "Preliminary design of a 352 MHz Drift Tube Linac with External Focusing", PS/RF/Note 97-18.
[3.16] D.A. Swenson, J. Stovall, "PARMILA", LANL Report MP-3-19.
[3.17] C. Benvenuti, D. Boussard, S. Calatroni, E. Chiaveri, J. Tückmantel, "Production and Test of 352 MHz Niobium Sputtered Reduced-Beta Cavities", CERN-SL 97-63 RF.
[3.18] K. Halbach, R.F. Holsinger, "SUPERFISH – A Computer Program for Evaluation of RF Cavities with Cylindrical Symmetry", Particle Accelerators 7 (4), 213-222.
[3.19] D.Boussard, E Chiaveri, G. Geschonke, J.Tuckmantel. "Preliminary Parameters of a Proton Linac Using the LEP2 RF System when Decommissioned", SL RF Technical Note 96-4.
[3.20] E. Brigant, E. Haebel, E. Mahner, "The quadrupole resonator, design considerations and layout of a new instrument for the RF characterization of superconducting surface samples", Proceedings of the EPAC Conference, Stockholm, 1998.
[3.21] E. Chiaveri, E. Haebel, E. Mahner, J.M. Tessier, "The Quadrupole Resonator: Construction, RF System, Field Calculations and First Applications", Proceedings of the EPAC Conference, Stockholm, 1998.
[3.22] D.V.Gorelov and P.N.Ostroumov, "LANA Computer Code For Design and Beam Dynamics Simulation in Ion Linacs", Proc. of the 1996 European Particle Accelerator Conference, Sitges (1996).
[3.23] J.-M. Tessier, "Field Stabilization in Superconducting Cavities in Pulsed Mode", Ph.D. thesis, Paris XI Orsay, 1996.
[3.24] K.R. Crandall, "TRACE-3D Documentation", LANL Report LA-1154-MS.
[3.25] LEP Design report, Vol. III, CERN-AC/96-01 (LEP2).
[3.26] L.Scherk, "An Improved Value for the Electron Affinity of the Negative Hydrogen Ion", Can. J. Physics, Vol. 57, p558, 1979.
[3.27] A.Jason, D.Hudgings, O. van Dyck, "Neutralisation of H^- Beam by Magnetic Stripping", IEEE Trans. Nucl. Sci., vol. NS-28, June 1981, p2704.
[3.28] R.Hutson, "Theoretical Study of H^- stripping with Wiggler Magnet", Proc. of the 1991 Part. Acc. Conference, San Francisco (1991).

Section 4

[4.1] R. Cappi, R.Garoby, S. Hancock, M. Martini, J.P. Riunaud, K. Schindl, H. Schönauer, "The PS as LHC Proton Source: Results of the two-week Beam Test in December 93", CERN/PS 94-11 (DI), 1994.
[4.2] R. Cappi, R.Garoby, S. Hancock, M. Martini, J.P. Riunaud, "Measurement and Reduction of Transverse Blow-up induced by Space Charge Effects", Proc. of the Part. Acc. Conf., Washington, May 1993, p.3570.
[4.3] J. Gareyte, "Requirements of the LHC on its injectors", Particle Accelerators, Vol.58, Numbers 1-4, (1997), pp53-61.
[4.4] The European Spallation Source Study, Volume III, The ESS Technical Study, ESS-96-53-M (1996), p.3-23.
[4.5] F.W. Jones, G.H. Mackenzie, H. Schönauer, "ACCSIM – A Program to Simulate the Accumulation of Intense Proton Beams", Proc. of the 14th International Conference on High Energy Accelerators, Tsukuba, Japan, 1989, in Particle Accelerators 31:199 (1990).
[4.6] C. Prior, "The Longitudinal Tracking Code TRACK1D", RAL Report, 1996.
[4.7] P. Knaus, "Simulation of Longitudinal Micro-Bunch Dynamics", Proc. of the Workshop on Space Charge Physics in High Intensity Hadron Rings, Shelter Island, NY, May 1998, AIP Conf. Proc. 448, p.379.

Section 5

[5.1] "ESS A Next Generation Neutron Source for Europe", J. Kjems, A.D. Taylor, J.L. Finney, H. Lengeler, U. Steigenberger, eds., Volume I, The European Spallation Source, ESS-96-53-M, March 1997, page 6.

[5.2] idem., Volume II, pages 5 and 72, and R. Scherm, PTB Braunschweig, private communication.

[5.3] H. Schönauer, "The PSB as a Compressor Ring for the Superconducting 2 GeV Linac with LHC Cavities", CERN-PS internal note PS/CA/Note 98-24.

[5.4] NSAC Long Range Plan, DOE/NSF Nuclear Science Advisory Committee, February 1996, http://pubweb.bnl.gov/~nsac/.

[5.5] "Scientific Opportunities with an Advanced ISOL Facility", Report by a Working Panel, November 1997, http://www.er.doe.gov/production/henp/isolpaper.pdf.

[5.6] "Nuclear Physics in Europe: Opportunities and Perspectives", NUPECC Report, November 1991.

[5.7] "Impact and Application of Nuclear Science in Europe: Opportunities and Perspectives", NUPECC, December 1994.

[5.8] "Nuclear Physics in Europe: Highlight and Opportunities", NUPECC Report, November 1991.

[5.9] "European Radioactive Beam Facilities, Statement by NUPECC", Report by Study Group, NUPECC, May 1993.

[5.10] E. Kugler, D. Fiander, B. Jonson, H. Haas, A. Przewloka, H.L. Ravn, D.J. Simon, K. Zimmer, and the ISOLDE Collaboration, "The new CERN-ISOLDE on-line mass-separator facility at the PS-Booster", Nucl. Instrum. Methods Phys. Res. B70 (1992) 41.